Nature Communications

https://doi.org/10.1038/s41467-026-69085-w

Article in Press

Constructing scalable hydrophobe–water micro-interfaces for catalyst-free generation of H_2O_2 via macroporous resins

Received: 22 April 2025

Accepted: 26 January 2026

Cite this article as: Gao, J., Zhou, K., Guo, X. *et al.* Constructing scalable hydrophobe–water micro-interfaces for catalyst-free generation of H_2O_2 via macroporous resins. *Nat Commun* (2026). https://doi.org/10.1038/s41467-026-69085-w

Jia Gao, Kai Zhou, Xiangliang Guo, Kairong Yang, Shuying Yang, Hua Su, Zhibing Zhang & Wei Wang

Constructing scalable hydrophobe–water micro-interfaces for catalyst-free generation of H_2O_2 via macroporous resins

Jia Gao[1], Kai Zhou[1], Xiangliang Guo[2], Kairong Yang[1], Shuying Yang[1], Hua Su[3]*, Zhibing Zhang[2]*, Wei Wang[1]*

[1] State Key Laboratory of Analytical Chemistry for Life Science, School of Chemistry and Chemical Engineering, ChemBIC (Chemistry and Biomedicine Innovation Center), Nanjing University, Nanjing 210023, China

[2] Key Laboratory of Mesoscopic Chemistry of Ministry of Education (MOE), School of Chemistry and Chemical Engineering, Nanjing University, Nanjing 210023, China

[3] School of Pharmacy, Nanjing University of Chinese Medicine, Nanjing 210023, China

*Email: suhua@njucm.edu.cn; zbzhang@nju.edu.cn; wei.wang@nju.edu.cn

Abstract

Catalyst-free production of H_2O_2 at hydrophobe–water micro-interfaces provides a sustainable synthesis route, yet its scalability remains challenging. We demonstrate that hydrophobic macroporous resins (MPRs) can serve as robust, metal-free platforms to construct scalable hydrophobic solid–water interfaces for continuous H_2O_2 generation, achieving a mass-normalized production rate of H_2O_2 as ~0.51 μmol g_{MPR}^{-1} h^{-1} and eventually ~1 mM-level accumulation of H_2O_2 after one week's stirring of the resin suspension under ambient atmosphere. Both macroporosity and hydrophobicity of MPRs are essential for the activity, and scale-up 1000 mL confirms practical feasibility. Mechanistic studies indicate that H_2O_2 forms predominantly via the oxygen reduction reaction (ORR), optimally at pH 9. This process requires no external light or electrical energy input, exhibits high salt tolerance, and is potentially compatible with renewable power sources. This work exemplifies how porous materials can enable sustainable, scalable chemical synthesis and updates the fundamental understanding of the microinterface reactivity.

Introduction

In the past decade, there has been a growing interest in a variety of aqueous interfaces, particularly hydrophobe–water interfaces such as gas–water, oil–water, and solid–water interfaces.[1-13] Intensive research has revealed that these interfaces possess unique chemical structures and exhibit distinct chemical reactivities from those observed in bulk solution chemistry.[14-19] For instance, studies have shown that in certain cases, microdroplets can significantly accelerate traditional chemical reactions by two to six orders of magnitude,[20-22] and even promote thermodynamically unfavorable reactions.[7,21,23-26] Very recently, particular attention has been paid to redox aqueous reactions at hydrophobe–water micrometer scale interfaces, specifically the spontaneous production of H_2O_2 in water microdroplets without the use of any conventional catalysts or external energy sources such as light or electricity.[8-10,27] This cutting-edge topic was first reported by Zare's group in 2019 and has since sparked wide active investigation into water microdroplets. Although the underlying mechanism has not been fully understood, this phenomenon offers new insights into the unique properties of aqueous interfaces and presents a new method for producing H_2O_2 under mild conditions.[28] As an indispensable chemical in various fields such as chemical synthesis, energy, environment, and human health, current industrial production of H_2O_2 heavily relies on the energy-intensive anthraquinone oxidation method, which generates large amounts of organic waste and frequently necessitates the use of expensive noble metal catalysts.[29] In comparison, the microdroplet-driven H_2O_2 generation from earth-abundant water is environmentally friendly and sustainable.

As experimental and theoretical studies continue to suggest that the generation of H_2O_2 in water microdroplets occurs at the hydrophobe–water interface, a consensus has emerged that expanding such interfaces could greatly enhance overall interfacial reactivity.[30] One promising strategy involves dispersing hydrophobic micro- or nanoparticles in bulk water to create extensive reactive sites. However, the high interfacial energy between water and hydrophobic materials presents a significant challenge in achieving stable and scalable interfaces. This is often accompanied with spontaneous agglomeration of the hydrophobic entities in aqueous environments, resulting in a decrease in the overall contact area with water and a drastic reduction in the chemical reactivity at the hydrophobe–water interface.[31,32] As a result, air-water microdroplets prepared by pneumatic spraying or condensation typically have a limited lifetime of only a few milliseconds due to evaporation or coalescence, resulting in a relatively low equilibrium concentration of H_2O_2 in the presence of O_2 (~ 1 μM after a complete removement of O_3) and a limited yield of H_2O_2.[8-10] As an alternative, dynamic water-in-oil microdroplets (prepared by ultrasonic irradiation of a mixture of oil and water) have been reported to produce a higher concentration of H_2O_2 (10 mM after one hour of reaction).[33] However, there are concerns about whether the detected H_2O_2 was entirely produced at the oil–water interface,[28] as vigorous ultrasonic irradiation can also produce H_2O_2 through mechanisms such as cavitation effects or ozone reaction.[34-36] Additionally, Wang's group has recently reported an interesting solid–liquid contact electrification method at the fluorine polymer–water interface, which can also lead to the formation of H_2O_2 with a rate of hundreds of μM per hour.[37,38] Recently, Choi, Zare, and coworkers further extended this concept and developed a continuous flow column reactor packed with poly(tetrafluoroethylene) (PTFE) microparticles. Under continuous ultrasonic operation, a high H_2O_2 production rate up to 10.7 mM h^{-1} was achieved by circulating the effluent.[39] However, this method is limited in its sustainability for green synthesis of H_2O_2 from H_2O, as it is mainly restricted to fluorine-containing polymers (a kind of forever chemicals that are lowly dispersible in water) and relies on vigorous energy input such as ultrasonic irradiation or ball milling.[40-42] Therefore, achieving scalable hydrophobe–water micro-interfaces for sustainable synthesis of H_2O_2 remains a challenge.

In our previous study,[30] by confining water microdroplets into an array of glass microwells on a chip, which were fabricated by photolithography, we observed a continuous production of H_2O_2 until reaching an equilibrium concentration in one hour's lifetime of droplets. Our findings also showed that the rate of spontaneous generation of H_2O_2 was directly proportional to the surface-to-volume ratio (S/V) of the water microdroplets. This led us to the idea of constructing similar structures that could capture a large number of water microdroplets with high S/V values, using easily accessible and inexpensive materials.

Macroporous resins (MPRs), a kind of off-the-shelf and metal-free porous solid adsorbent, are commonly used in industrial water treatment for the removal of inorganic and organic pollutants.[43-45] They are typically created by polymerizing monomers in the presence of pore-forming agents. One of the key features of MPRs is their hierarchical porous structure, ranging from several nanometers to tens of microns, which provides a large surface area for adsorption. Our attention was drawn to the potential of MPRs to "grasp" water through porous structures and create a large number of long-lasting water microdroplets within their porous structures. This could be particularly beneficial if the walls of the pores in MPRs are intrinsically hydrophobic, as it would allow for the creation of stable and thus scalable hydrophobe–water micro-interfaces for the generation of H_2O_2. These water microdroplets also have the advantage of intimate communication with the bulk water, which differs from our previous separated water microdroplets confined in an array of glass microwells. We expect that the continuous diffusion of H_2O_2 produced at these hydrophobe–water micro-interfaces into the bulk water could ultimately provide a sustainable manner to produce and accumulate H_2O_2 under mild conditions.

Hence, in this study, we screened a range of commercially available MPRs with polystyrene/divinylbenzene (PS-DVB) backbones. Our findings revealed that it is possible to create scalable hydrophobe–water micro-interfaces using hydrophobic MPRswith facilitated production of H_2O_2 from H_2O and O_2. It was found that, without the use of ultrasonic irradiation and surfactants, a production rate of H_2O_2 of ~0.51 μmol g_{MPR}^{-1} h^{-1} and an eventual ~1 mM-level accumulation of H_2O_2 after one week's stirring under ambient atmosphere could be achieved in hydrophobic MPRs. This exceeds the previously reported H_2O_2 concentration of ~1 μM formed in air–water microdroplets without ultrasonication.[8-10,30] As a proof of concept, scaling the system to a 1000 mL reaction volume was also conducted, demonstrating its practical scalability. Further investigations have elucidated that both the porous structure and the hydrophobic nature of the pore walls in MPRs are crucial for the generation of H_2O_2. Mechanistic study verified that the formed H_2O_2 originates from oxygen reduction reaction (ORR), with optimal performance at pH 9. The existence of multiple reactive species (e.g., ·OH, e^-, $\cdot O_2^-$) indicated that interfacial charge separation and electron transfer drive the underlying H_2O_2 formation.

Results

Screening and characterization of macroporous resins (MPRs) for H_2O_2 production

Prior to measurements, we conducted a general pre-treatment procedure on the obtained MPRs with different sizes, rigidities, and chemical compositions (Supplementary Table 1 and Supplementary Fig. 1) to remove the impurities from the industrial synthesis of MPRs (more details can be found in the Methods Section). To evaluate the potential of commercially available MPRs for the construction of scalable hydrophobe–water micro-interfaces, we mixed 20 mg of the treated MPRs (Supplementary Fig. 2) with 0.6 mL of deionized water in a 4 mL polypropylene (PP) tube. To ensure proper dispersion of the MPRs in the water, we added a polytetrafluoroethylene (PTFE) or glass-capped magnetic stir bar to the tube and used a magnetic stirring apparatus (Fig. 1). After a period of time, the resulting mixture was centrifuged and filtered through a filter membrane. For the most extensively studied XAD-1180N MPRs in this work, scanning electron microscopy (SEM) revealed that they had a wide range of sizes (1–10 μm) and highly heterogeneous porous structures after experiments (Supplementary Fig. 2b). The liquid supernatant was then analyzed using a widely used fluorescence method to determine the concentration of H_2O_2, based on the horseradish peroxidase (HRP)-catalyzed oxidation of Amplex Red (AR) by H_2O_2 (Supplementary Fig. 3).[46] In addition, we also performed a UV–vis absorbance method using potassium titanium (IV) oxalate (PTO method, Supplementary Fig. 4 & Supplementary Fig. 5)[8,9] to verify the results.

According to the proposed procedures, we conducted a screening of both macroporous and microporous resins and monitored their rate of H_2O_2 generation under identical conditions. In order to provide a comparison, we also tested several non-porous materials, including polystyrene (PS), PTFE, SiO_2, and agarose gel. Our results indicate that porous materials generally exhibit a higher rate of H_2O_2 generation compared to non-porous materials with the same mass, as shown in Fig. 2A. Additionally, it was observed that hydrophobic MPRs displayed higher rates of H_2O_2 generation compared to their hydrophilic counterparts (Fig. 2A). It is noteworthy that three MPRs with crosslinked PS-DVB structures, *i.e.*, XAD-1180N, XAD-2 and XAD-4, exhibited the highest initial production rate of H_2O_2 (~ 17 μM h^{-1} or ~ 0.51 μmol g^{-1} h^{-1}) among all the materials that were tested. These three materials had broad size distributions in the range of 1–10 μm, with main porous sizes of 30 nm, 9 nm, and 10 nm, respectively (Supplementary Table 1). Furthermore, we continuously monitored the generation of H_2O_2 in several materials, including XAD-1180N, D101, XAD-7, and non-porous PS (Supplementary Fig. 6). For instance, during a kinetics test of XAD-1180N, we observed a steady increase in H_2O_2 concentration, eventually reaching an accumulated concentration of 1 mM over the course of a week

(Fig. 2B). In view of the specificity of PTO method and HPR-based fluorescence method, which may respond to other reactive oxygen species (ROS), we also performed another ^{1}H NMR measurements of the reaction solution using the method proposed by Bax and colleagues.[47] As shown in Supplementary Fig. 7, the ^{1}H NMR spectrum of both the 100 μM H_2O_2 standard and the reaction solution exhibits a singlet peak at a chemical shift of 10.97 ppm, which is characteristic of H_2O_2. Further quantitative integration of these singlet peaks revealed the same concentration of H_2O_2 as that measured by the PTO method and the fluorescence method. Therefore, the reported values of 1 mM indeed reflect the concentration of H_2O_2 rather than other ROS species. Importantly, this value exceeds those previously reported in sprayed or condensed water microdroplets by two to three orders of magnitude (1 mM versus ~ 1 μM).[8-10] It should also be noted that although generation rate of H_2O_2 for these MPRs is much lower than that of PTFE–water interface under vigorous ultrasonic irradiation (~ 17 μM h^{-1} for MPRs vs. ~ 300 μM h^{-1} for PTFE),[37,39] the advantages of less intensive energy input for long-term accumulation of H_2O_2 at ambient conditions and high tolerance to various salts (please see the following Fig. 5A) for these MPRs endows it more easily to be scaled up for a wide range of applications.

Considering that various radical initiators are typically used in the synthesis of macropolymers, we were concerned about whether their gradual release and subsequent reaction with water contributed to the high accumulated concentration of H_2O_2. In order to address this concern, we repeatedly determined the generation rate of H_2O_2 by recycling the used XAD-1180N MPRs nine times. This process involved multiple cycles of washing, drying, redispersion, and reaction. Interestingly, as shown in Fig. 2C, the generation rate of H_2O_2 remained nearly constant, indicating that the observed H_2O_2 generation was an intrinsic behavior of XAD-1180N and not caused by the residual impurities in the MPRs.

Notably, during the dispersion of the tested materials into water, three distinct dispersion behaviors were observed. To facilitate observation, after a certain time of stirring, various mixtures were promptly transferred from the original PP tubes to glass vials and photographs were taken (Fig. 2D). A dynamic recording of the dispersed process of XAD-1180N MPRs, PTFE, and SiO_2 over a four-hour stirring period is also shown in Supplementary Fig. 8. Hydrophilic SiO_2, Si_3N_4, ZnO, and other hydrophilic resins, which exhibited negligible production of H_2O_2 (Fig. 2A), demonstrated uniform dispersion in water following several seconds to minutes of stirring (right bottle in the inset picture of Fig. 2D). In contrast, nonporous and hydrophobic materials like PTFE, PS, and polystyrene-divinylbenzene (PS-DVB) exhibited a reduced capacity for dispersion in water (middle bottle in the inset picture of Fig. 2D) and demonstrated a comparatively low production rate of H_2O_2. However, the dispersion process of porous resins, particularly hydrophobic MPRs, was found to be entirely different (Supplementary Fig. 8). Upon contact with water, these materials initially rose to the water surface, a behavior commonly observed in other hydrophobic materials devoid of porous structures. However, with continued stirring, they gradually transformed into a dispersed emulsion with the water. After four hours of stirring, it was observed that the dispersed state could be sustained for tens of minutes without significant bulk phase separation (left bottle in the inset picture of Fig. 2D). A more quantitative assessment of the dispersion process of these three types of materials was conducted by monitoring the time-evolved scattering intensity of mixture solutions at the bottom of the sample vials, further confirming the different dispersion behavior of XAD-1180 N MPRs (Fig. 2D). The effect of stirring speed on the dispersity of MPR over time and the generation rate of H_2O_2 was also examined (Supplementary Fig. 9). It was observed that increasing the stirring speed resulted in a faster dispersion of MPR in water, leading to a higher average generation rate of H_2O_2. These observations highlight the distinctive characteristics of hydrophobic MPRs, indicating that MPRs can create a large number of long-lasting water microdroplets with high S/V values by “grasping” water into their porous structures. As stirring continues, the gradual extrusion of water into their pores may give rise to a substantial number of water microdroplets, which remain connected to the bulk water.

Therefore, considerable hydrophobe–water interfaces were established, which could support the impressive concentration of H_2O_2 generation.

In our previous study, we demonstrated that the generation rate of H_2O_2 in single water microdroplets at the oil–water interface is positively proportional to the S/V values of the water microdroplets–a finding that supports the hypothesis of H_2O_2 formation occurring at the hydrophobe–water micro-interfaces.[30] This finding also motivated the present investigation into the correlation between the surface area of hydrophobic MPRs and their rate of H_2O_2 generation. To this end, we adopted the widely used Brunauer-Emmett-Teller (BET) gas adsorption method to quantify the specific surface area of several hydrophobic MPRs (Supplementary Table 2). The BET analysis revealed a broad pore size distribution in these materials, ranging from several to tens of nanometers (as shown in the BET pore distribution of XAD-1180N shown in Supplementary Fig. 10). This is consistent with the heterogeneity of the porous structures of XAD-1180N, as observed in the SEM characterization (Supplementary Fig. 2b). This suggests that the water droplets confined within these pores may also exhibit a significant heterogeneity. Additionally, the BET results showed that among the materials tested, the most active MPRs (XAD-1180N, XAD-2, and XAD-4) exhibited slightly larger surface areas per unit mass, with values of 10.40, 13.80, and 14.24 m^2, respectively (Supplementary Table 2). After normalizing the rate of H_2O_2 generation by surface area, a linear correlation was observed with a constant of 1.3 μM m^{-2} h^{-1} (or 0.78 nmol m^{-2} h^{-1}, Fig. 1E), confirming that H_2O_2 generation occurs at the hydrophobic surface of MPRs. Interestingly, it was found that several non-porous materials showed higher surface area-normalized activity of H_2O_2 generation, that is, ~0.42 μmol m^{-2} h^{-1} for PS-DVB, ~0.02 μmol m^{-2} h^{-1} for PS, and ~0.004 μmol m^{-2} h^{-1} for PTFE (Supplementary Fig. 11). However, due to the high S/V values of MPRs per unit mass, MPRs exhibit significantly greater mass-normalized reactivity than these non-porous materials (~0.511 μmol g^{-1} h^{-1} for MPR, ~0.019 μmol g^{-1} h^{-1} for PS-DVB, ~0.015 μmol g^{-1} h^{-1} for PS, ~0.002 μmol g^{-1} h^{-1} for PTFE), making them more suitable as building blocks in the construction of scalable hydrophobe–water micro-interfaces for H_2O_2 generation. Notably, the surface-normalized H_2O_2 generation rate determined for MPRs was approximately 600 times lower than the value previously reported for microwell-confined water microdroplets (0.78 nmol m^{-2} h^{-1} vs. 0.462 μmol m^{-2} h^{-1}).[30] This discrepancy suggests that a substantial fraction of the hydrophobic surface area in the MPRs didn't contribute to the generation of H_2O_2, likely due to mass transfer limitations of water molecules into the hydrophobic inner pores of the MPR microspheres. This hypothesis is supported by subsequent atmospheric experiments (discussed in the following mechanism section) and consistent with a Cassie-Baxter wetting state of porous materials[48-50], in which air or O_2 remains trapped within the porous structures of the MPRs (the cartoon of the top-right panel of Fig. 1). We propose that pre-saturation with water vapor–a method successfully applied to introduce water into the nanopores of activated carbon[51]–could enhance water penetration into hydrophobic MPR pores and mitigate this limitation in future applications.

Influence of MPR hydrophobicity on the activity of H_2O_2 generation

To further elucidate the critical role of hydrophobic surfaces in the generation of H_2O_2, two complementary *in situ* surface modification strategies were implemented. First, the hydrophobic resin XAD-1180N MPR was functionalized with hydrophilic dextran polymers (Fig. 3A & Supplementary Fig. 12a). As the amount of dextran precursors used during the surface functionalization process increased, a marked reduction in the hydrophobicity of XAD-1180N was observed, which correlated with a systematic decrease in the H_2O_2 generation rate, as shown in Fig. 3B. For example, after treatment with 10% dextran precursors, the apparent water contact angle of XAD-1180N MPRs decreased from the original 148.5° to 133.0°, accompanied by a 60% reduction in the H_2O_2 generation rate. This inverse relationship underscores the high sensitivity of interfacial reactivity to the wettability of the MPR–water interfaces. It is noteworthy that the apparent contact angles measured herein may exceed the intrinsic Young's contact angles due to air or O_2

entrapment within the porous framework of MPRs (*i.e.*, Cassie-Baxter state[48-50]). Nevertheless, the consistent trend of enhanced H_2O_2 generation with increasing surface hydrophobicity remains robust, as evidenced by the pronounced decline in activity upon hydrophilic modification. In the converse experiment, hydrophobic modification was applied to an inherently hydrophilic material. Sengarose, a highly porous and hydrophilic agarose gel, was grafted with hydrophobic butyl groups via its surface hydroxyl groups (Fig. 3C & Supplementary Fig. 12b). In contrast to the hydrophilic treatment of XAD-1180N, the introduction of butyl groups led to a gradual increase in H_2O_2 production as the degree of grafting increased, as shown in Fig. 3D. Together, these two sets of experiment provide coherent and compelling evidence that surface hydrophobicity is a pivotal factor governing H_2O_2 generation at the MPR–water micro-interfaces. Moreover, the consistent trends observed upon both hydrophilic and hydrophobic functionalization strongly suggest that the production of H_2O_2 is not an artifact of residual impurities in the MPRs, but is intrinsically mediated by the properties of the solid–water micro-interfaces.

Recently, Zare and colleagues reported ~1 μM H_2O_2 formation in air–water microdroplets after excluding contributions from ultrasonic effect and ozone reaction,[10] whereas we observed a much higher concentration of ~ 1 mM H_2O_2 at the MPR–water interfaces, though the latter is less hydrophobic than air. This discrepancy does not contradict the positive correlation between hydrophobicity and H_2O_2 production. The low concentration of H_2O_2 in air–water microdroplets arises from their transient lifetime (milliseconds to seconds), which limits sustained accumulation of H_2O_2 despite potentially high interfacial reactivity. In contrast, the porous structure of MPRs stabilizes water microdroplets for extended periods (e.g., one week), facilitating continuous H_2O_2 generation and accumulation. Regarding the influence of surface wettability on H_2O_2 production, Mishra et al. recently demonstrated that hydrophilic surfaces (e.g., galvanic metals such as Mg, Al) can exhibit enhanced H_2O_2 production via a single dissolved oxygen reduction mechanism at the metal–water interface.[52] This implies that distinct mechanisms may operate in different systems, each with specific interfacial requirements. We suggest that the critical underlying feature is the interface's capacity to facilitate charge separation and electron transfer—not hydrophobicity or hydrophilicity per se. In our case, hydrophobicity serves as an empirical and practical descriptor within comparable MPR systems, where it correlates reliably with H_2O_2 production efficiency.

Previous results in water microdroplets also showed that the presence of oxygen gas can significantly promote the formation of H_2O_2 by consuming the generated electrons.[10] We thus evaluated the influence of gas atmosphere on H_2O_2 generation. Under argon or nitrogen saturation (achieved through rigorous degassing), H_2O_2 production decreased tenfold compared to air or O_2 conditions (Supplementary Fig. 13a), aligning with earlier microdroplet reports. However, when only the aqueous phase was purged with N_2—while leaving the MPR pores undegassed—H_2O_2 generation remained comparable to that in air-saturated systems. This indicates that MPRs retain substantial trapped air/O_2 within their porous framework, maintaining the Cassie-Baxter wetting state[48-50] (inferred from the stabilized gas retention, though not directly visualized). Consequently, the hydrophobe–water micro-interfaces in our system comprise both MPR–water and air–water interfaces, possibly collectively enabling 1 mM-level H_2O_2 accumulation.

Mechanistic insights into H_2O_2 generation in the MPR system

Having confirmed the key role of macroporous features and hydrophobic surfaces in H_2O_2 generation, we proceeded to investigate the underlying reaction mechanism, as mechanistic insight is essential for guiding future optimization and scalable implementation of MPR-based systems. Isotope experiments ($H_2{}^{18}O$ and $^{18}O_2$) were first conducted to trace the origin of oxygen atoms in the H_2O_2 produced.[37,53,54] As illustrated in Fig. 4A, oxygen isotopes incorporated into H_2O_2 can be detected via high-resolution mass spectrometry after cleavage of 4-

carboxyphenylboronic acid. While minimal ^{18}O incorporation occurred under O_2/H_2O or $O_2/H_2{}^{18}O$ conditions (mass spectrometric peak at m/z of 139.0286 is barely visible in Fig. 4B), strong labeling was observed with $^{18}O_2/H_2O$, confirming molecular oxygen as the predominant oxygen source. Moreover, the concentration of H_2O_2 generated under the condition of $^{18}O_2/H_2O$ nearly remained the same as that of normal O_2/H_2O conditions (Supplementary Fig. 14), which rules out significant O_3 involvement in the MPR system. These results robustly support oxygen reduction reaction (ORR) as the primary pathway for H_2O_2 formation in the presence of air or O_2 atmosphere for the MPR system, rather than the recombination of hydroxyl radicals (·OH) from water oxidation reaction (WOR)[8] in the MPR system. To further examine the participation of reducing equivalents (e.g., electrons or hydrogen atoms) in the formation of H_2O_2—a phenomenon reported in air–water microdroplets—we employed a fluorogenic assay based on the reduction of resazurin (RZR) to fluorescent resorufin (RSF) (Supplementary Fig. 13b). Under an argon atmosphere, we stirred an aqueous solution of XAD-1180N MPRs and RZR for twelve hours and observed a higher formation of RSF compared to when the experiment was conducted under air conditions. Consistently, adding the electron scavenger p-benzoquinone (PBQ) to MPR–water mixtures markedly suppressed H_2O_2 production (Fig. 4C). These findings confirm the presence of reductive species during H_2O_2 generation, such as electrons or hydrogen atoms, which would have been scavenged by O_2 in the presence of air (see Supplementary Fig. 13b). Additionally, superoxide anion radical ($\cdot O_2^-$) scavenger experiments revealed that superoxide dismutase (SOD) can suppress the H_2O_2 generation in the MPR system, while further introduction of SOD inhibitors, N, N-diethyldithiocarbamate (DDC) and KN_3, can restore the generation of H_2O_2 (Fig. 4D and Supplementary Fig. 15a-b). The presence of $\cdot O_2^-$ was also confirmed by a nitrotetrazolium blue chloride (NBT) reduction test, in which stirring the aqueous mixtures of MPR and NBT in the presence of O_2 yielded a characteristic blue-purple formazan product (Supplementary Fig. 15c-d). Together, these data validate the dominant ORR pathway for H_2O_2 formation in MPR systems under aerated conditions: $O_2 \rightarrow \cdot O_2^- \rightarrow H_2O_2$ (Fig. 4I).

We next examined the influence of solution pH (ranging from 4 to 12, buffered by 0.1 M phosphate) on H_2O_2 generation. The MPR system exhibited higher activity under alkaline conditions, with an optimum at pH 9 (Fig. 4E). This mild alkaline preference differs from the acidic optimum reported for ultrasound-mediated water-in-oil microdroplets (another hydrophobe–water interface) where ORR pathway dominated the H_2O_2 formation under acidic settings,[54] but similar to Christian George's recent observations of enhanced H_2O_2 generation in alkaline hydrophobe–water droplets.[55]

Using electron paramagnetic resonance (EPR) spectroscopy with the spin trap 5,5-dimethyl-1-pyrroline N-oxide (DMPO) as a spin trap, we detected the characteristic quadruplet signal of DMPO-·OH in MPR–water mixtures (Fig. 4F). We further quantified ·OH production using the fluorogenic probe terephthalic acid (TPA), which reacts with ·OH to form highly fluorescent 2-hydroxyterephthalic acid (hTPA, Supplementary Fig. 16a). The fluorescence intensity increased continuously over 12 hours, confirming the sustained generation of ·OH radicals. Quantitative analysis revealed that ·OH was produced concurrently with H_2O_2, but at a concentration approximately 200 times lower (Fig. 4G and Supplementary Fig. 16b-c). Adding the ·OH radical scavenger isopropanol (IPA) into the reaction mixture slightly increased H_2O_2 production (Fig. 4H). A strong interfacial electric field (EF, 10^9 V/m), localized to a region of several angstroms at the hydrophobe–water interfaces, has been proposed to drive charge separation and potentially oxidize adsorbed hydroxide ions (OH^-) or water to hydroxyl radicals (·OH), which could subsequently recombine to form H_2O_2.[4,6-10,15-19] Several recent studies by other groups have questioned the role of such strong interfacial EFs in the formation of ·OH from OH^-.[11-13,52,56-59] While our results confirm ·OH formation in the MPR–water system, we emphasize that detection of ·OH radicals alone does not prove water oxidation reaction (WOR), because ·OH may also originate from catalytic decomposition of H_2O_2 via ORR pathway—a well-documented secondary reaction in redox systems.

Although the ORR pathway for H_2O_2 formation in the MPR system is established and the hydrogen in H_2O_2 unequivocally comes from H_2O, the source of electrons (or reducing equivalents) remains unresolved. In a recent study on sonicated emulsified water microdroplets, Rodriguez-Lopez and coworkers also identified ORR as the dominant route for H_2O_2 formation, but noted that the origin of the reducing power remains unclear.[60] Current literature suggests two possible electron-donation pathways at aqueous microinterfaces: sole oxidation of solid surface (as proposed by Mishra Mishra and coworkers[12,52]) or oxidation of water (WOR, as suggested by Zare and George groups[8-10,15,16]), as shown in Fig. 4I. Both pathways would result in surface oxidation of the organic MPR framework, and X-ray photoelectron spectroscopy (XPS) analysis revealed slight oxidation of post-reaction MPRs (Supplementary Fig. 17). Directly distinguishing these mechanisms is challenging due to interfacial complexity and the lack of real-time electron-tracking tools.

To probe whether WOR contributes under our conditions, we designed an experiment in which O_2 was replaced with the electron acceptor PBQ and H_2O was replaced by 100% $H_2{}^{18}O$ (Supplementary Fig. 18). If WOR occurred, $H_2{}^{18}O_2$ should form and be detectable via isotopic analysis. After two weeks of stirring under a nitrogen atmosphere, a low concentration of H_2O_2 (i.e., ~10 μM) was detected with the HRP-AR fluorometric method, but high-resolution mass spectrometry showed no detectable ^{18}O incorporation into the peroxide product. Thus, under these experimental conditions, we cannot confirm a significant WOR contribution in our MPR system. Potential limitations—such as background interference from the resin matrix or adsorption of the probe—may have affected sensitivity. Further methodological refinements will be required to conclusively resolve the electron-transfer pathway. In summary, our mechanistic investigation establishes ORR as the dominant route for H_2O_2 formation at MPR–water interfaces under aerated conditions, while the role of water oxidation remains unverified with the present data. These insights not only clarify the reaction pathway in our system but also contribute to the ongoing discussion on redox mechanisms at hydrophobic microinterfaces.

Robustness and scalability of the MPR-based H_2O_2 production process

Further, the effects of various salts on the generation of the MPR system were examined. As shown in Fig. 5A, the introduction of 1 M Na_2SO_4 and 1 M NaCl did not affect the generation of H_2O_2 compared to pure water, while that of phosphate solution, tap water, and simulated seawater only slightly decreased the activity. This is significantly different from that of PTFE–water interface under vigorous ultrasonic irradiation, wherein addition of 1M NaCl leads to a >90% decrease of H_2O_2 generation.[37] This high tolerance of MPRs to various salts makes it a potential candidate for application in long-term oceangoing voyages, such as disinfection of ships, whilst the exact mechanism needs further study. Another interesting finding is that when XAD-1180N MPR was dispersed in a CO_2-saturated water and stirred for six hours, the average H_2O_2 generation rate was similar to that of normal conditions, which may be due to the strong buffering capacity of the MPR (Fig. 5A). Furthermore, it was found that even after thermal treatment at 300 °C for four hours, the activity of MPR remained unaffected (Fig. 5B). These results demonstrate the robustness of the MPR system for constructing scalable hydrophobe–water micro-interfaces for catalyst-free synthesis of H_2O_2.

Subsequently, the potential for expanding these hydrophobe–water micro-interfaces, which are based on MPRs for H_2O_2 generation, to a larger-scale reaction volume was considered, an essential step toward potential industrial application. As a proof of concept, the reaction volume was scaled from 0.6 mL to 1000 mL, representing an amplification factor of ~1800, and the generation of H_2O_2 was monitored at ambient conditions. To facilitate the dispersion of MPRs, a mechanical mixer was utilized, as illustrated in Fig. 5C. Due to the well-defined particle size of

MPRs (1–10 μm), the generated H_2O_2 could be easily extracted via low-cost and straightforward filtration. Over the course of one week, stirring of aqueous mixtures of MPRs, a continuous accumulation of H_2O_2 was visually confirmed using a commercial H_2O_2 test strip (Fig. 5D), reaching a final accumulated H_2O_2 concentration exceeding 100 μM. Quantified analysis further demonstrated a nearly linear increase in H_2O_2 concentration during this period, with the resultant accumulated concentration reaching ca. 150 μM (Fig. 5E). This outcome validates the operational viability of MPRs-based water micro-interfaces for the scalable synthesis of H_2O_2. Although the accumulated H_2O_2 concentration decreased by approximately sevenfold compared to the small-scale (600 μL) system, this reduction is likely attributable to the lower stirring efficiency in the larger setup. As indicated in Supplementary Fig. 9, improved dispersion through optimized agitation enhances H_2O_2 generation. However, for practical large-scale applications, milder stirring with a larger propeller could be employed, potentially coupled with sustainable energy sources such as wind, hydraulic, or tidal power, making the system particularly promising for remote or marine operations. Extending the reaction time is expected to enable accumulation up to ~1 mM H_2O_2 (Fig. 5E). Further enhancements in H_2O_2 yield could be achieved through physical or chemical modification of MPRs (e.g., material process engineering) or via reactor optimization to improve the dispersion of MPRs and the mass transfer of H_2O/O_2. In this proof-of-concept scalable experiment, a resin loading of 100 g/L was used; higher loadings may be employed in future applications given the low cost, wide availability, and excellent recyclability of MPRs (e.g., over nine cycles without significant loss of activity; Fig. 2C). Notably, this process operates without energy-intensive inputs such as sonication or photo/electrochemical excitation and exhibits high tolerance to salts and elevated temperatures. Thus, the proposed MPR system represents a promising and sustainable strategy for scalable H_2O_2 production.

Discussion

In this work, we present a sustainable strategy for hydrogen peroxide (H_2O_2) production by employing the off-the-shelf, metal-free hydrophobic macroporous resins (MPRs) in water to provide scalable and tunable hydrophobe–water micro-interfaces. These interfaces enable the direct synthesis of H_2O_2 generation from H_2O and O_2 without conventional catalysts, external light or electrical energy input, or chemical additives. Simply stirring an aqueous suspension of MPRs – specifically those containing polystyrene/divinylbenzene (PS-DVB) backbones, such as XAD-1180N, XAD-2, and XAD-4 – achieves a mass-normalized H_2O_2 production rate of up to ~0.51 μmol g_{MPR}^{-1} h^{-1} under ambient atmosphere, leading to an eventual ~1 mM-level accumulation of H_2O_2 within one week. This process operates without ultrasonication, surfactants, or custom-synthesized new materials.

As a proof-of-concept of scalability, operation in a 1000 mL reactor yielded an accumulated H_2O_2 concentration of ~150 μM after one week. Systematic investigations shows that both the macroporous architectures and hydrophobic surface characteristics of MPRs are essential for efficient H_2O_2 generation. This system performs optimally under alkaline conditions (pH 9) and maintains high tolerance to various salts, highlighting its robustness for diverse aqueous environments. Mechanistically, isotope labeling experiments ($H_2{}^{18}O$ and $^{18}O_2$) confirm that molecular oxygen is the predominant oxygen source for H_2O_2 formation, with negligible O_3 involvement, supporting the oxygen reduction reaction (ORR) as the dominant pathway. The detection of reactive intermediates (e.g., ·OH, e^-, $\cdot O_2^-$) further indicates that interfacial charge separation and electron transfer drive continuous H_2O_2 formation. These findings resemble those reported in air–water microdroplet systems, but are achieved here through readily scalable solid–water interfaces, bringing new insights into microdroplet and micro-interface chemistry. Nevertheless, further research is needed to provide clearer insights into the latter aspects. Owing to its operational simplicity, compatibility with renewable energy sources (e.g., wind, hydraulic, or tidal power), salt tolerance, and minimal infrastructure requirements, the MPR-based system offers a promising route toward decentralized, green H_2O_2 production, especially in remote or marine settings.

More broadly, this work demonstrates how engineered porous materials can be used to create functional solid–liquid microscale interfaces for sustainable chemical synthesis, opening new avenues for applying interfacial phenomena in continuous-flow and industrially relevant systems.

Methods

Dispersing porous resins in water for H_2O_2 generation

Commercially available macroporous and microporous resins microspheres of various sizes and compositions (Supplementary Fig. 1 and Supplementary Table 1) were ground into powders with a typical particle size of 1–10 µm. The powders were washed by sonication in ethanol for 30 min, centrifuged, and this process was repeated three times. After vacuum-drying at 60 °C for 24 h, 20 mg of powder was dispersed in 0.6 mL of deionized water (DIW) in a 4 mL polypropylene (PP) tube containing a glass- or PTFE-coated magnetic stir bar (1500 rpm). Following stirring, the reaction mixture was centrifuged at 21,100 x *g* for 5 min (Legend Micro 21R, Thermo Fisher Scientific) and filtered through a <0.10 µm membrane. The resulting particle-free filtrate was used for H_2O_2 quantification by fluorescence (HRP-AR method) or absorbance (PTO method) assays, as detailed below. To provide a comparison, several other non-porous materials, including PS, PTFE, SiO_2, and agarose gel, were also tested by the same method.

Fluorescence-based H_2O_2 quantification (HRP-AR method)

A working solution containing 10 nM HRP, 100 µM AR, and 10 mM phosphate buffer (pH 7.4) was prepared. For the assay, 20 µL of sample or H_2O_2 standard (1–100 µM) solution was mixed with 180 µL working solution in a 1.5 mL PP tube, vortexed for 15 s, and incubated for 3 min. A 100 µL aliquot was transferred to a black 96-well plate, and fluorescence was measured (λ_{ex}=530 nm, λ_{ex}=590 nm, gain=35) on a Biotek Synergy LX microplate reader. Kinetic measurements confirmed that the HRP-catalyzed conversion of AR to resorufin was complete within 3 min and remained stable (Supplementary Fig. 3a-b). The assay showed linear response for final H_2O_2 concentrations of 0.1–10 µM (Supplementary Fig. 3c). Samples exceeding this range were diluted with DIW prior to analysis.

Absorbance-based H_2O_2 quantification (PTO method)

An equal volume (200 µL) of 10 mM PTO solution and H_2O_2 standard solution (1–200 µM) were mixed in a 1.5 mL PP tube, vortexed for 15 s, and incubated at room temperature for 2 min. Subsequently, a 200 µL aliquot was transferred to a transparent 96-well microplate. Absorbance spectra were recorded from 350 to 650 nm using a microplate reader (Supplementary Fig. 4a). Calibration curves were generated by plotting the absorbance at 400 nm against H_2O_2 concentration. A linear calibration curve ($R^2 > 0.99$) was obtained in the range of 10–200 µM, with a detection limit of ~5 µM (Supplementary Fig. 4b-c). Filtered samples were analyzed identically.

^{1}H NMR measurement of H_2O_2

H_2O_2 was quantified via ^{1}H NMR spectroscopy following a reported protocol.[47] After 120 h's stirring of an aqueous dispersion of XAD-1180N MPRs, filtered reaction mixtures were spiked with 2-(N-morpholino)ethanesulfonic acid (MES) from a 50 mM in D_2O stock to a final concentration of 1 mM, and the pH was adjusted to 6.0 ± 0.05 using a calibrated pH meter. A commercial H_2O_2 standard (100 µM) was processed identically as a reference. Spectra were acquired on a Bruker Avance III HD 600 MHz spectrometer equipped with a CPBBO cryoprobe. Results were cross-validated using the HRP-AR and PTO assays (Supplementary Fig. 7).

Hydrophobic modification of agarose gel

Butyl groups were grafted onto the hydroxyl chains of agarose via a published procedure (Supplementary Fig. 12a).[61] Commercial agarose gel (containing 20% ethanol) was washed three times with deionized water, followed by solvent exchange with anhydrous dioxane. To ensure complete dehydration, the gel was suspended in anhydrous dioxane, agitated for 10 min, and centrifuged; this process was repeated five times. Subsequently, 1 mL of the dehydrated gel was mixed with 1 mL of anhydrous dioxane and 20 µL of boron trifluoride etherate ($BF_3 \cdot Et_2O$) catalyst, shaken at 100 rpm for 5 min, then treated with varying amounts of n-Butyl glycidyl ether at 45 °C for 45 min under shaking (100 rpm). Finally, the modified gel was washed alternately with dioxane and water (three cycles), followed by seven washes with DIW to remove residual reagents. This yielded butyl-agarose gels with tunable hydrophobicity.

Hydrophilic modification of macroporous resins

Hydrophilic dextran chains were grafted onto MPR phenyl rings via a two-step Friedel–Crafts/nucleophilic substitution route (Supplementary Fig. 12b).[62] First, MPR beads were washed with ethanol, dried at 60 °C for 12 h, and swollen in carbon disulfide (CS2) for 12 h. Aluminum chloride ($AlCl_3$, 1.2 eq. based on styrene units) and 2-chloromethylacetyl chloride (1.0 eq., dissolved in CS_2) were added. The reaction was stirred at 50 °C for 4 h. The intermediate MPR-Cl was washed, filtered, and dried. Second, MPR-Cl (1.0 g) was swollen in anhydrous DMSO (10 mL) for 12 h. Separately, dextran (MW 10,000, 0.4 g) was dissolved in anhydrous DMSO (40 mL) containing sodium hydride (0.236 g) to deprotonate hydroxyl groups. The activated dextran solution was mixed with the swollen MPR-Cl, and tetrabutylammonium bromide (TBAB, 0.5 eq.) was added as a phase-transfer catalyst, and the mixture was reacted at 65 °C for 24 h to yield the hydrophilic-modified resin.

Contact angle measurement and BET analysis

Contact angles were measured on an optical contact angle meter.[63, 64] Powder samples were immobilized on double-sided adhesive tape, and excess powder was removed by repeated pressing to form a uniform thin layer. A 3 µL droplet of deionized water was dispensed onto the sample surface using a computer-controlled needle. Images were captured immediately, and contact angles were calculated via the ellipse-fitting method in the instrument software. Specific surface areas and pore size distributions were determined via nitrogen adsorption-desorption isotherms using the BET method.[65,66]

Atmosphere control experiment

Anaerobic experiments were conducted in a glovebox filled with high-purity nitrogen (O_2<0.1 ppm). All components were rigorously degassed to eliminate atmospheric interference (Supplementary Fig. 13). Ultrapure water was deoxygenated following a modified protocol by Mishra et al.[52]: water was heated to boiling in a sealed beaker, followed by purging with nitrogen gas for 45 minutes. Dissolved oxygen in the resulting water was quantified using a Hach dissolved-oxygen meter and was consistently below 0.1 ppm. The water was then transferred and sealed in a vial within the glovebox. Dry MPR powder underwent five vacuum/nitrogen refill cycles in the glovebox antechamber, then continuous evacuation (>10 h) to remove the maximum amount of residual gas trapped within the pores. Sample assembly was performed entirely within the inert atmosphere.

For O_2-rich conditions, resin and a magnetic stir bar were loaded into a reaction tube fitted with a three-way valve. The system was purged to remove trapped gas, and oxygen-saturated deionized water was injected through the valve. An oxygen balloon was attached to the top of the tube to maintain a positive oxygen pressure during the reaction (Supplementary Fig. 13).

Oxygen isotope labeling experiments and MS analysis

Oxygen-atom origins in H_2O_2 were traced using $H_2{}^{18}O$ and $^{18}O_2$ via mass spectrometry (MS) after derivatization with 4-Carboxyphenylboronic acid (CPBA), which reacts stoichiometrically with H_2O_2 to yield 4-hydroxybenzoic acid (4-HBA).[54] Incorporation of an ^{18}O atom results in a characteristic +2 Da m/z shift in the 4-HBA spectrum. High-resolution MS analysis was performed on an Agilent 6540 Q-TOF. For $H_2{}^{18}O$ experiments, MPR powders (20 mg) were stirred in 600 µL of 30% $H_2{}^{18}O$ for 100 h, filtered, and the supernatant was incubated with 2 mM CPBA for 1 h prior to MS analysis. For $^{18}O_2$ experiments, reaction assembly was carried out in a nitrogen-filled glovebox. Degassed water and MPR powder were placed in a 4 mL PP tube. This tube and a 1 L gas bag filled with $^{18}O_2$ were sealed together inside a transparent 2.5 L barrier pouch. To initiate the reaction, the gas bag was opened within the sealed pouch to create an $^{18}O_2$ atmosphere, and the reaction tube was uncapped. The system was stirred for 100 h, followed by the same workup and analysis procedures used for the $H_2{}^{18}O$ experiment.

Quantitative determination of ·OH

Hydroxyl radicals (·OH) were quantified using terephthalic acid (TPA) as a fluorogenic probe.[54] Non-fluorescent TPA reacts specifically with ·OH to form the highly fluorescent 2-hydroxyterephthalic acid (hTPA). XAD-1180N MPRs were suspended in a 2 mM aqueous TPA solution and stirred. After the reaction, the supernatant was collected, and fluorescence intensity was recorded on a Hitachi F-7000 spectrophotometer (λ_{ex}=315 nm, λ_{em}=425 nm). ·OH concentrations were derived from a calibration curve constructed from authentic hTPA standards (<1000 nM) (Supplementary Fig. 16).

Scalable experiment

A large-scale batch reaction was performed with 100 g of XAD-1180N MPRs dispersed in 1.1 L of DIW under ambient conditions. Mixing was achieved using a mechanical stirrer (Lichen, China) operated at 500 rpm with glass beads added to aid dispersion. Over one week, 2 mL aliquots were periodically collected, centrifuged, and analyzed using commercial H_2O_2 test strips (Merck, Germany; Product No. 1.10011.0001), with results cross-verified by the HRP-AR assay described above.

Data Availability Statement

All data that support the findings of this study are available from the corresponding author upon request. Source data are provided with this paper.

References

1. Du, Q., Superfine, R., Freysz, E. & Shen, Y. R. Vibrational spectroscopy of water at the vapor/water interface. *Phys. Rev. Lett.* **70**, 2313–2316 (1993).

2. Björneholm, O., Hansen, M. H., Hodgson, A., Liu, L.-M., Limmer, D. T., Michaelides, A., Pedevilla, P., Rossmeisl, J., Shen, H., Tocci, G., Tyrode, E., Walz, M.-M., Werner, J. & Bluhm, H. Water at interfaces. *Chem. Rev.* **116**, 7698–7726 (2016).

3. Ruiz-Lopez, M. F., Francisco, J. S., Martins-Costa, M. T. C. & Anglada, J. M. Molecular reactions at aqueous interfaces. *Nat. Rev. Chem.* **4**, 459–475 (2020).

4. Shi, L., LaCour, R. A., Qian, N., Heindel, J. P., Lang, X., Zhao, R., Head-Gordon, T. & Min, W. Water structure and electric fields at the interface of oil droplets. *Nature*, **640**, 87–93 (2025).

5. Pullanchery, S., Kulik, S., Rehl, B., Hassanali, A. & Roke, S. Charge transfer across C–H · · · O hydrogen bonds stabilizes oil droplets in water. *Science* **374**, 1366–1370 (2021).

6. Xiong, H., Lee, J. K., Zare, R. N. & Min, W. Strong electric field observed at the interface of aqueous microdroplets. *J. Phys. Chem. Lett.* **11**, 7423–7428 (2020).

7. Xing, D., Meng, Y., Yuan, X., Jin, S., Song, X., Zare, R. N. & Zhang, X. Capture of hydroxyl radicals by hydronium cations in water microdroplets. *Angew. Chem. Int. Ed.* **61**, e202207587 (2022).
8. Lee, J. K., Walker, K. L., Han, H. S., Kang, J., Prinz, F. B., Waymouth, R. M., Nam, H. G. & Zare, R. N. Spontaneous generation of hydrogen peroxide from aqueous microdroplets. *Proc. Natl Acad. Sci. USA* **116**, 19294–19298 (2019).
9. Lee, J. K., Han, H. S., Chaikasetsin, S., Marron, D. P., Waymouth, R. M., Prinz, F. B. & Zare, R. N. Condensing water vapor to droplets generates hydrogen peroxide. *Proc. Natl Acad. Sci. USA* **117**, 30934–30941 (2020).
10. Mehrgardi, M. A., Mofidfar, M. & Zare, R. N. Sprayed water microdroplets are able to generate hydrogen peroxide spontaneously. *J. Am. Chem. Soc.* **144**, 7606–7609 (2022).
11. Chen, C. J. & Williams, E. R. Are hydroxyl radicals spontaneously generated in unactivated water droplets? *Angew. Chem. Int. Ed.* **63**, e202407433 (2024).
12. Eatoo, M. A. & Mishra, H. Disentangling the roles of dissolved oxygen, common salts, and pH on spontaneous hydrogen peroxide production in water: no O_2, no H_2O_2. *J. Am. Chem. Soc.* **147**, 35392–35400 (2025).
13. Shirley, J. C., Ng, Z. X., Chiang, K. Y., Nagata, Y., Litman, Y., Hazrah, A. S. & Bonn, M. Reevaluating anomalous electric fields at the air-water interface: a surface-specific spectroscopic survey. *J. Am. Chem. Soc.* **147**, 46163–46173 (2025).
14. LaCour, R. A., Heindel, J. P., Zhao, R. & Head-Gordon, T. The role of interfaces and charge for chemical reactivity in microdroplets. *J. Am. Chem. Soc.* **147**, 6299–6317 (2025).
15. Li, K., Guo, Y., Nizkorodov, S. A., Rudich, Y., Angelaki, M., Wang, X., An, T., Perrier, S. & George, C. Spontaneous dark formation of OH radicals at the interface of aqueous atmospheric droplets. *Proc. Natl Acad. Sci. USA* **120**, e2220228120 (2023).
16. Angelaki, M., Carreira Mendes Da Silva, Y., Perrier, S. & George, C. Quantification and mechanistic investigation of the spontaneous H_2O_2 generation at the interfaces of salt-containing aqueous droplets. *J. Am. Chem. Soc.* **146**, 8327–8334 (2024).
17. Heindel, J. P., Hao, H., LaCour, R. A. & Head-Gordon, T. Spontaneous formation of hydrogen peroxide in water microdroplets. *J. Phys. Chem. Lett.* **13**, 10035–10041 (2022).
18. Hao, H., Leven, I. & Head-Gordon, T. Can electric fields drive chemistry for an aqueous microdroplet? *Nat. Commun.* **13**, 280 (2022).
19. Chen, X., Xia, Y., Zhang, Z., Hua, L., Jia, X., Wang, F. & Zare, R. N. Hydrocarbon degradation by contact with anoxic water microdroplets. *J. Am. Chem. Soc.* **145**, 21538–21545 (2023).
20. Xue, L., Chen, W., Zheng, P., Geng, J., Zhang, F., Li, X., Zhang, Z. & Hu, X. Catalyst-free oxidation of styrene to styrene oxide using circulating microdroplets in an oxygen atmosphere. *J. Am. Chem. Soc.* **146**, 26909–26915 (2024).
21. Wei, Z., Li, Y., Cooks, R. G. & Yan, X. Accelerated reaction kinetics in microdroplets: overview and recent developments. *Annu. Rev. Phys. Chem.* **71**, 31–51 (2020).
22. Vannoy, K. J., Edwards, M. Q., Renault, C. & Dick, J. E. An electrochemical perspective on reaction acceleration in microdroplets. *Annu. Rev. Anal. Chem.* **17**, 149–171 (2024).
23. Lee, J. K., Samanta, D., Nam, H. G. & Zare, R. N. Spontaneous formation of gold nanostructures in aqueous microdroplets. *Nat. Commun.* **9**, 1562 (2018).
24. Yuan, X., Zhang, D., Liang, C. & Zhang, X. Spontaneous Reduction of Transition Metal Ions by One Electron in Water Microdroplets and the Atmospheric Implications. *J. Am. Chem. Soc.* **145**, 2800–2805 (2023).
25. Xia, D., Zhang, H., Ju, Y., Xie, H.-b., Su, L., Ma, F., Jiang, J., Chen, J. & Francisco, J. S. Spontaneous degradation of the "forever chemicals" perfluoroalkyl and polyfluoroalkyl substances (pfass) on water droplet surfaces. *J. Am. Chem. Soc.* **146**, 11266–11271 (2024).
26. Jiang, Q., Xia, D., Li, X., Zhang, H., Yin, R., Xie, H., Xie, H. b., Jiang, J., Chen, J. & Francisco, J. S. Rapid N_2O formation from N_2 on water droplet surfaces. *Angew. Chem. Int. Ed.* **64**, e202421002 (2025).
27. Li, J., Xia, Y., Song, X., Chen, B. & Zare, R. N. Continuous ammonia synthesis from water and nitrogen via contact electrification. *Proc. Natl. Acad. Sci. U.S.A.* **121**, e2318408121 (2024).

28. Nguyen, D., Lyu, P. & Nguyen, S. C. Experimental and thermodynamic viewpoints on claims of a spontaneous H_2O_2 formation at the air–water interface. *J. Phys. Chem. B* **127**, 2323–2330 (2023).

29. Campos-Martin, J. M., Blanco-Brieva, G. & Fierro, J. L. G. Hydrogen peroxide synthesis: an outlook beyond the anthraquinone process. *Angew. Chem. Int. Ed.* **45**, 6962–6984 (2006).

30. Zhou, K., Su, H., Gao, J., Li, H., Liu, S., Yi, X., Zhang, Z. & Wang, W. Deciphering the kinetics of spontaneous generation of H_2O_2 in individual water microdroplets. *J. Am. Chem. Soc.* **146**, 2445–2451 (2024).

31. Sun, M., Lu, Q., Wang, Z. L. & Huang, B. Understanding contact electrification at liquid-solid interfaces from surface electronic structure. *Nat. Commun.* **12**, 1752 (2021).

32. Kim, Y., Ding, H. & Zheng, Y. Investigating water/oil interfaces with opto-thermophoresis. *Nat. Commun.* **13**, 3742 (2022).

33. Lee, K., Lee, H.-R., Kim, Y. H., Park, J., Cho, S., Li, S., Seo, M. & Choi, S. Q. Microdroplet-mediated radical polymerization. *ACS Cent. Sci.* **8**, 1265–1271 (2022).

34. Musskopf, N. H., Gallo, A. Jr., Zhang, P., Petry, J. & Mishra, H. The air–water interface of water microdroplets formed by ultrasonication or condensation does not produce H_2O_2. *J. Phys. Chem. Lett.* **12**, 11422–11429 (2021).

35. Nguyen, D. & Nguyen, S. C. Revisiting the effect of the air–water interface of ultrasonically atomized water microdroplets on H_2O_2 formation. *J. Phys. Chem. B* **126**, 3180–3185 (2022).

36. Gallo Jr, A., Musskopf, N. H., Liu, X., Yang, Z., Petry, J., Zhang, P., Thoroddsen, S., Im, H. & Mishra, H. On the formation of hydrogen peroxide in water microdroplets. *Chem. Sci.* **13**, 2574–2583 (2022).

37. Zhao, J., Zhang, X., Xu, J., Tang, W., Lin Wang, Z. & Ru Fan, F. Contact-electro-catalysis for direct synthesis of H_2O_2 under ambient conditions. *Angew. Chem. Int. Ed.* **62**, e202300604 (2023).

38. Berbille, A., Li, X.-F., Su, Y., Li, S., Zhao, X., Zhu, L. & Wang, Z. L. Mechanism for generating H_2O_2 at water-solid interface by contact-electrification. *Adv. Mater.* **35**, 2304387 (2023).

39. Lee, K., Bose, S., Song, X., Choi, S. Q. & Zare, R. N. Continuous flow contact electrocatalysis for hydrogen peroxide production. *J. Phys. Chem. C* **129**, 6254–6261 (2025).

40. Wang, Z., Dong, X., Tang, W. & Wang, Z. L. Contact-electro-catalysis (CEC). *Chem. Soc. Rev.* **53**, 4349–4373 (2024).

41. Wang, Z., Dong, X., Li, X. F., Feng, Y., Li, S., Tang, W. & Wang, Z. L. A contact-electro-catalysis process for producing reactive oxygen species by ball milling of triboelectric materials. *Nat. Commun.* **15**, 757 (2024).

42. Wang, Z., Berbille, A., Feng, Y., Li, S., Zhu, L., Tang, W. & Wang, Z. L. Contact-electro-catalysis for the degradation of organic pollutants using pristine dielectric powders. *Nat. Commun.* **13**, 130 (2022).

43. Aiken, G. R., Thurman, E. M., Malcolm, R. L. & Walton, H. F. Comparison of XAD macroporous resins for the concentration of fulvic acid from aqueous solution. *Anal. Chem.* **51**, 1799–1803 (1979).

44. Kim, J., Kim, D., Gwon, Y. J., Lee, K.-W. & Lee, T. S. Removal of sodium dodecylbenzenesulfonate by macroporous adsorbent resins. *Materials* **11**, 1324 (2018).

45. Shi, C., Li, Y., Li, X., Zhao, X., Ma, X., Zhou, X., Cui, Y., Ma, S., Xu, W. & Ren, C. Preparation of macroporous high adsorbent resin and its application for heavy metal ion removal. *Chem. Select* **6**, 9038–9045 (2021).

46. Zhou, M., Diwu, Z., Panchuk-Voloshina, N. & Haugland, R. P. A stable nonfluorescent derivative of resorufin for the fluorometric determination of trace hydrogen peroxide: applications in detecting the activity of phagocyte NADPH oxidase and other oxidases. *Anal. Biochem.* **253**, 162–168 (1997).

47. Kakeshpour, T. & Bax, A. NMR characterization of H_2O_2 hydrogen exchange. *J. Magn. Reson.* **333**, 107092 (2021).

48. Cassie, A. B. D. & Baxter, S. Wettability of porous surfaces. *Trans. Faraday Soc.* **40**, 546–550 (1944).

49. Whyman, G., Bormashenko, E. & Stein, T. The rigorous derivation of Young, Cassie–Baxter and Wenzel equations and the analysis of the contact angle hysteresis phenomenon. *Chem. Phys. Lett.* **450**, 355–359 (2008).

50. Marmur, A., Della Volpe, C., Siboni, S., Amirfazli, A. & Drelich, J. W. Contact angles and wettability: towards common and accurate terminology. *Surf. Innov.* **5**, 3–8 (2017).

51. Shi, Y., Mu, H., You, J., Han, C., Cheng, H., Wang, J., Hu, H. & Ren, H. Confined water–encapsulated activated carbon for capturing short-chain perfluoroalkyl and polyfluoroalkyl substances from drinking water. *Proc. Natl Acad. Sci. USA* **120**, e2219179120 (2023).

52. Eatoo, M. A. & Mishra, H. Busting the myth of spontaneous formation of H_2O_2 at the air–water interface: contributions of the liquid–solid interface and dissolved oxygen exposed. *Chem. Sci.* **15**, 3093–3103 (2024).

53. Chen, B., Xia, Y., He, R., Sang, H., Zhang, W., Li, J., Chen, L., Wang, P., Guo, S., Yin, Y., Hu, L., Song, M., Liang, Y., Wang, Y., Jiang, G. & Zare, R. N. Water–solid contact electrification causes hydrogen peroxide production from hydroxyl radical recombination in sprayed microdroplets. *Proc. Natl Acad. Sci. USA* **119**, e2209056119 (2022).

54. Zhou, X., Du, S., Zhang, W. & Zheng, B. Deciphering the mechanism of hydrogen peroxide formation in ultrasound-mediated water-in-oil microdroplets. *Chem. Sci.* **16**, 6450–6457 (2025).

55. Angelaki, M., d'Erceville, J., Donaldson, D. J. & George, C. pH affects the spontaneous formation of H_2O_2 at the air–water interfaces. *J. Am. Chem. Soc.* **146**, 25889–25893 (2024).

56. Martins-Costa, M. T. & Ruiz-López, M. F. Probing solvation electrostatics at the air–water interface. *Theor. Chem. Acc.* **142**, 29 (2023).

57. Gong, K., Nandy, A., Song, Z., Li, Q.-S., Hassanali, A., Cassone, G., Banerjee, S. & Xie, J. Revisiting the enhanced chemical reactivity in water microdroplets: the case of a Diels-Alder reaction. *J. Am. Chem. Soc.* **146**, 31585–31596 (2024).

58. Chen, C. J. & Williams, E. R. A source of the mysterious m/z 36 ions identified: implications for the stability of water and unusual chemistry in microdroplets. *ACS Cent. Sci.* **11**, 622–628 (2025).

59. Chen, C. J. & Williams, E. R. An alternative explanation for ions put forth as evidence for abundant hydroxyl radicals formed due to the intrinsic electric field at the surface of water droplets. *Anal. Chem.* **97**, 17687–17695 (2025).

60. Asserghine, A., Baby, A., N'Diaye, J., Romo, A. I. B., Das, S., Litts, C. A., Jain, P. K. & Rodríguez-López, J. Dissolved oxygen redox as the source of hydrogen peroxide and hydroxyl radical in sonicated emulsive water microdroplets. *J. Am. Chem. Soc.* **147**, 11851–11858 (2025).

61. Zhang, N., Wang, J., Ye, J., Zhao, P. & Xiao, M. Oxyalkylation modification as a promising method for preparing low-melting-point agarose. *Int. J. Biol. Macromol.* **117**, 696–703 (2018).

62. Bowes, B. D. & Lenhoff, A. M. Protein adsorption and transport in dextran-modified ion-exchange media. III. Effects of resin charge density and dextran content on adsorption and intraparticle uptake. *J. Chromatogr. A* **1218**, 7180–7188 (2011).

63. Li, Y., Pham, J. Q., Johnston, K. P. & Green, P. F. Contact angle of water on polystyrene thin films: effects of CO2 environment and film thickness. *Langmuir* **23**, 9785–9793 (2007).

64. Brown, P. S. & Bhushan, B. Mechanically durable liquid-impregnated honeycomb surfaces. *Sci. Rep.* **7**, 6083 (2017).

65. Bardestani, R., Patience, G. S. & Kaliaguine, S. Experimental methods in chemical engineering: specific surface area and pore size distribution measurements—BET, BJH, and DFT. *Can. J. Chem. Eng.* **97**, 2781–2791 (2019).

66. Allanas, E., Rahman, A., Arlin, E. & Prasetyanto, E. A. Study surface area and pore size distribution on synthetic zeolite X using BET, BJH and DFT methods. *J. Phys. Conf. Ser.* **2019**, 012094 (2021).

Acknowledgements

We acknowledge the financial support from the National Key Research and Development Program (No. 2024FYA1509600, W.W.) and the National Natural Science Foundation of China (Nos. 22474060, H.S.; 22327803, W.W.).

Author Contributions Statement

All authors have given approved to the final version of the manuscript. H.S., Z.B.Z and W.W. designed the project. H.S., J.G., and W.W. wrote the paper. J.G., K.Z., and H.S. carried out most of the experiments and analyzed the data. X.L.G., K.R.Y., and S.Y.Y. participated in discussing the manuscript. W.W. conceived and supervised the project.

Competing Interests Statement

The authors declare no competing interests.

Figure Legends (for main text figures)

Fig. 1 Illustrated experimental procedures for using macroporous resins (MPRs) to create scalable hydrophobe–water micro-interfaces for H_2O_2 generation from H_2O and O_2. Scale bar, 500 μm. The top-right cartoon depicts the Cassie-Baxter state of MPRs during operation, in which a small amount of air or O_2 is trapped within the porous structures of the MPRs.

Fig. 2 Experimental demonstration of MPRs in the construction of scalable hydrophobe–water micro-interfaces for H_2O_2 generation. (A) The recorded initial generation rate of H_2O_2 in different materials tested, including MPRs, non-porous materials, and hydrophilic materials. These values were obtained by dispersing the same mass (20 mg) of each material into 0.6 mL of deionized water. The detailed chemical information of these tested materials can be found in Supplementary Table 1. (B) The kinetic curves of H_2O_2 generation monitored in XAD-1180N MPRs and the non-porous polystyrene (PS). (C) The recycled use of XAD-1180N MPRs for H_2O_2 generation. (D) Time-dependent dispersion profiles of XAD-1180N MPRs, PTFE, and SiO_2 in water over a four-hour stirring period, monitored via scattering intensity measurements. The inset picture shows the final dispersion state of each material after four hours. (E) The positive correlation of rates of H_2O_2 generation with the surface area of hydrophobic MPRs is normalized to their mass. Data in (A) and (B) are presented as mean ± standard deviation (n = 3 independent experiments).

Fig.3 Investigation of the role of the hydrophobic nature of the pore wall of MPRs in H_2O_2 generation. (A) Scheme of hydrophilic treatment of XAD-1180N MPRs by grafting dextran structures onto their phenyl rings. (B) The recorded rate of H_2O_2 generation for XAD-1180N MPRs at different degrees of hydrophilic treatment and their contact angles. (C) Scheme of hydrophobic modification of sengarose, a typical porous and hydrophilic agarose gel, by grafting hydrophobic butyl groups onto its hydroxyl groups. (D) The generation rate of H_2O_2 for sengarose at different levels of hydrophobic treatment and their contact angles. Data in (B) and (D) are presented as mean ± standard deviation (n = 3 independent experiments).

Fig.4 Deciphering the mechanism of H_2O_2 generation in the MPR–water system. (A) Illustration of isotope labeling of H_2O_2-promoted deborylation of 4-carboxyphenylboronic acid into 4-hydroxybenzoic acid. (B) High-resolution mass spectrometric analysis of 4-hydroxybenzoic acid products produced under O_2/H_2O, $O_2/H_2{}^{18}O$, and $^{18}O_2/H_2O$ conditions. (C) Effects of electron scavenger p-benzoquinone (PBQ) on H_2O_2 generation rate of XAD-1180N at normal (aerobic) conditions. (D) Confirmation of superoxide radical anions ($\cdot O_2^-$) through the use of superoxide dismutase (SOD) and its inhibitor N, N-diethyldithiocarbamate (DDC). (E) Comparison of H_2O_2 generation rates of XAD-1180N at different pH values in 100 mM phosphate buffer solution. DIW represents de-ionized water. (F) ESR trapping of hydroxyl radicals (·OH). (G) Quantification of time-evolved formation of ·OH radicals during the generation of H_2O_2, measured using terephthalic acid (TA) as a probe. (H) H_2O_2 Evolution in the presence of ·OH radical scavenger isopropanol (IPA) at varying concentrations. (I) Proposed pathway of H_2O_2 generation in the MPR–water system, involving interfacial charge separation, electron transfer, and formation of immediate species. ORR dominates H_2O_2 formation, while the source of

electrons remains unresolved. Two possible electron-donation pathways at aqueous microinterfaces are proposed: sole oxidation of the solid surface (path A) and oxidation of water (path B). Data in panels (D), (E), and (H) are presented as mean ± standard deviation (n = 3 independent experiments).

Fig.5 Robustness of the MPR system for catalyst-free generation of H_2O_2 from H_2O and O_2 at ambient conditions. (A) Effects of various salts (1 M Na_2SO_4, NaCl, Na_2HPO_4), tap water, and simulated seawater (3.5 wt% NaCl) on H_2O_2 production in the MPR system. (B) Thermal treatment of XAD-1180N at 300 and 350 °C for four hours showed negligible effects on H_2O_2 production activity, demonstrating the robustness of the MPR system for sustainable H_2O_2 synthesis. (C) Experimental setup for a proof-of-concept demonstration of a one-liter reaction volume containing 1.1 L of deionized water and 100 g of XAD-1180N MPRs for the continuous generation of H_2O_2. A 500-rpm mechanical mixer with some glass beads was used to facilitate the dispersion of MPRs in the water. (D) A continuous generation of H_2O_2 exceeding 100 μM during one week of stirring of the aqueous dispersion solution of MPRs, as verified by a commercial H_2O_2 test strip (Merck). For comparison, an aqueous solution containing 100 μM H_2O_2 is used as a reference. (E) Quantification of continuous H_2O_2 generation during one-week stirring of MPRs–water mixtures by HRP-AR assay. Data in (A) and (B) are presented as mean ± standard deviation (n = 3 independent experiments).

Editorial Summary

The catalyst-free production of H_2O_2 at solid-water interfaces provides a sustainable synthesis route, yet scalability remains challenging. Here the authors demonstrate that hydrophobic macroporous resins can serve as robust, metal-free platform to construct scalable and robust hydrophobe-water interfaces for continuous H_2O_2 generation.

Peer review information: *Nature Communications* thanks Himanshu Mishra, who co-reviewed with Muzzamil Eatoo; Ryan Sullivan; and Richard Zare for their contribution to the peer review of this work. A peer review file is available.

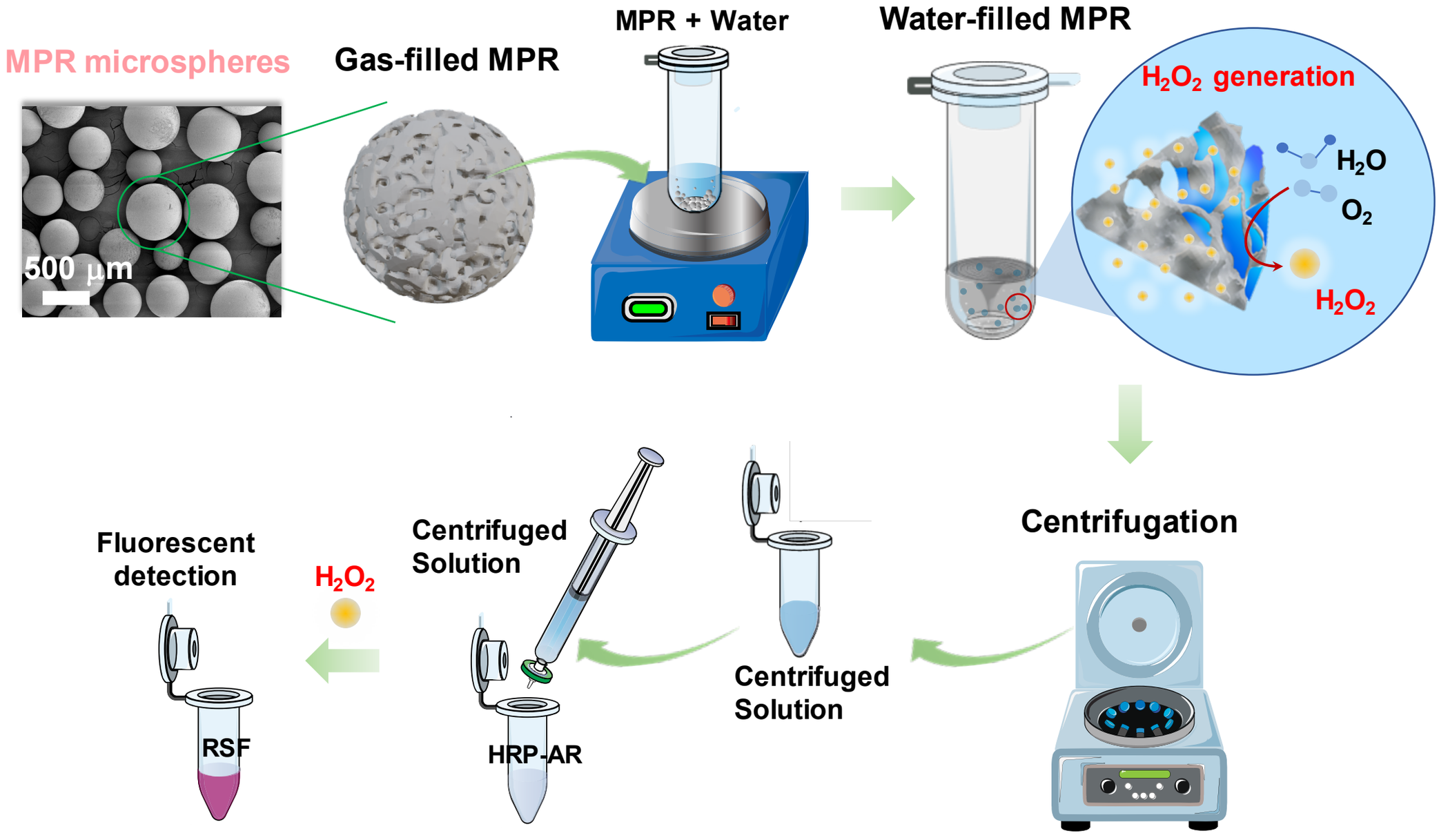
MPR microspheres
500 μm
Gas-filled MPR
MPR + Water
Water-filled MPR
H_2O_2 generation
H_2O
O_2
H_2O_2
Centrifugation
Centrifuged Solution
HRP-AR
Centrifuged Solution
H_2O_2
Fluorescent detection
RSF

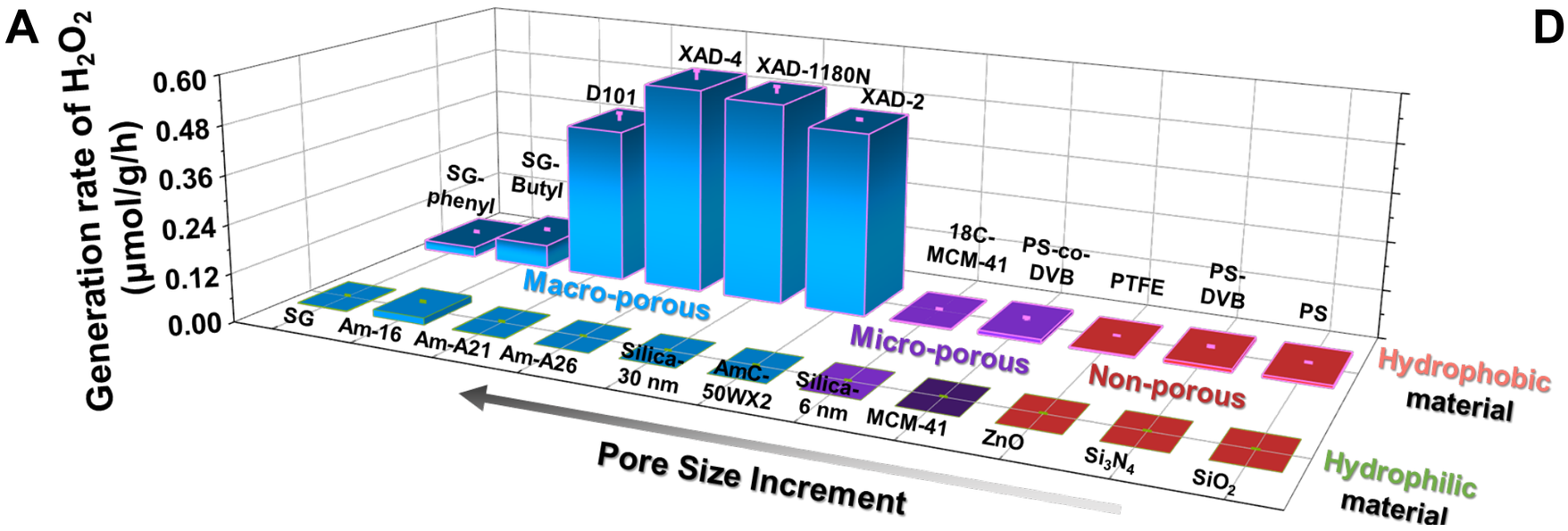
A
Generation rate of H_2O_2 (μmol/g/h)
0.60
0.48
0.36
0.24
0.12
0.00
XAD-4
XAD-1180N
XAD-2
D101
SG-phenyl
SG-Butyl
18C-MCM-41
PS-co-DVB
PTFE
PS-DVB
PS
SG
Am-16
Am-A21
Am-A26
Silica-30 nm
AmC-50WX2
Silica-6 nm
MCM-41
ZnO
Si_3N_4
SiO_2
Macro-porous
Micro-porous
Non-porous
Hydrophobic material
Hydrophilic material
Pore Size Increment

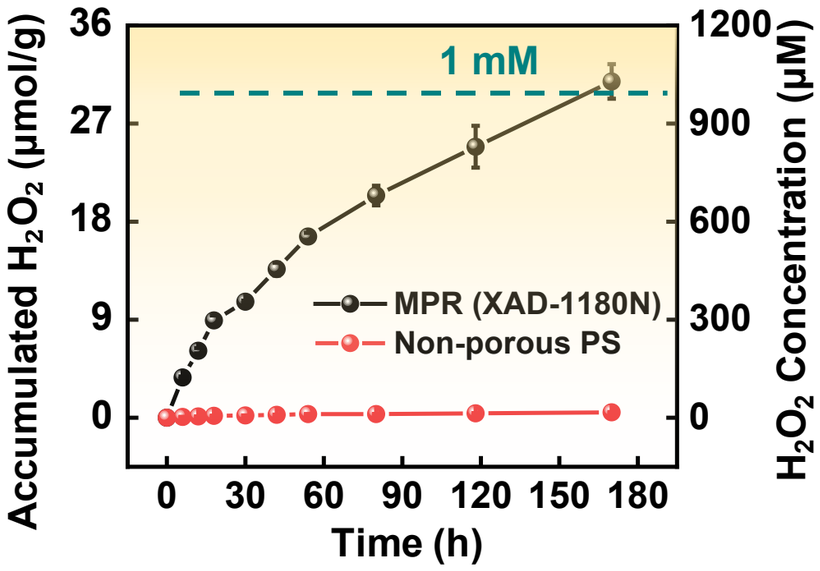
B
Accumulated H_2O_2 (μmol/g)
36
27
18
9
0
1200
900
600
300
0
H_2O_2 Concentration (μM)
1 mM
MPR (XAD-1180N)
Non-porous PS
0
30
60
90
120
150
180
Time (h)

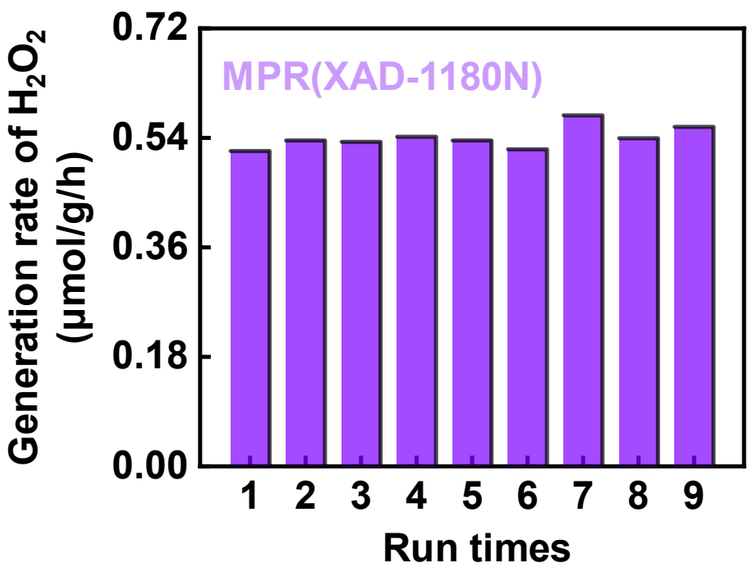
C
Generation rate of H_2O_2 (μmol/g/h)
0.72
0.54
0.36
0.18
0.00
MPR(XAD-1180N)
1
2
3
4
5
6
7
8
9
Run times

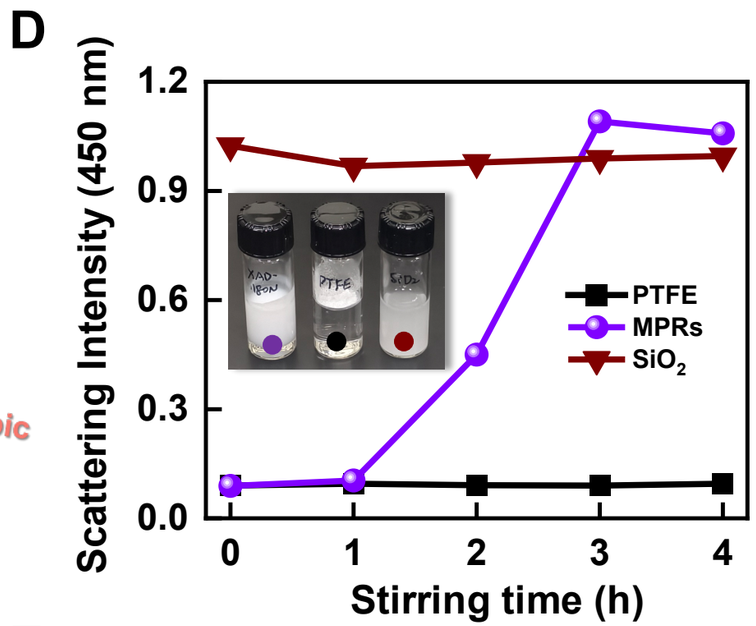
D
Scattering Intensity (450 nm)
1.2
0.9
0.6
0.3
0.0
PTFE
MPRs
SiO_2
0
1
2
3
4
Stirring time (h)

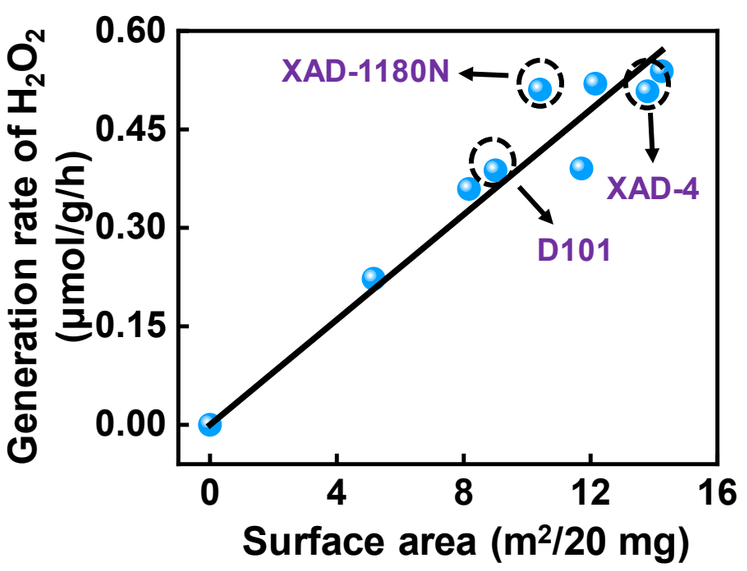
E
Generation rate of H_2O_2 (μmol/g/h)
0.60
0.45
0.30
0.15
0.00
XAD-1180N
XAD-4
D101
0
4
8
12
16
Surface area (m^2/20 mg)

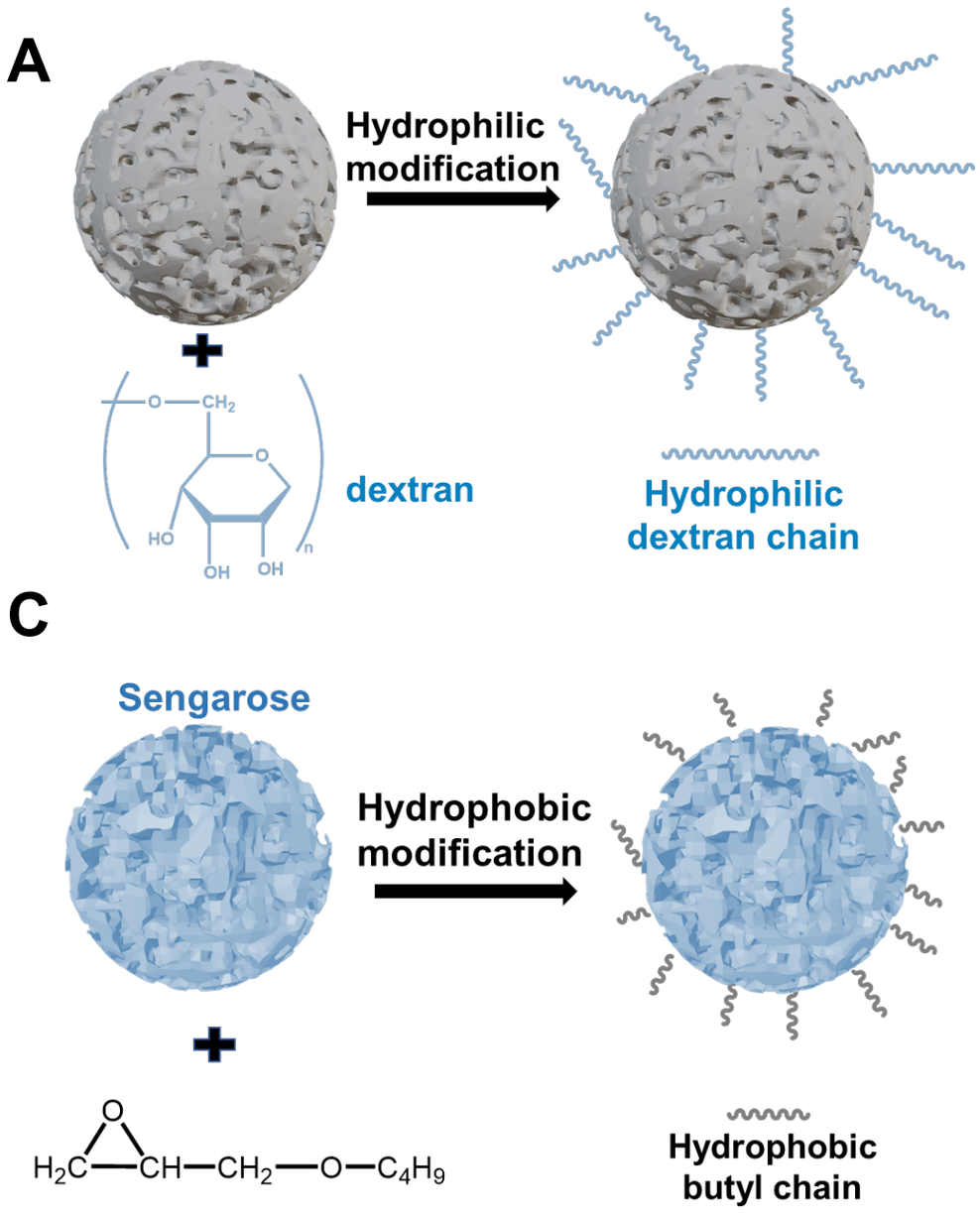
A
Hydrophilic modification
dextran
Hydrophilic dextran chain
C
Sengarose
Hydrophobic modification
Hydrophobic butyl chain
B
Generation rate of H_2O_2 (μmol/g/h)
0.72
0.54
0.36
0.18
0.00
149.5°
141.4°
133.0°
93.9°
Increased hydrophilicity
Bare XAD-1180N
Bare Dextran
5% Dextran
10% Dextran
Bare XAD-7
D
Generation rate of H_2O_2 (μmol/g/h)
0.036
0.027
0.018
0.009
0.000
Increased hydrophobicity
0:100
2:100
4:100
8:100
16:100
SG
SG-1
SG-2
SG-3
SG-4

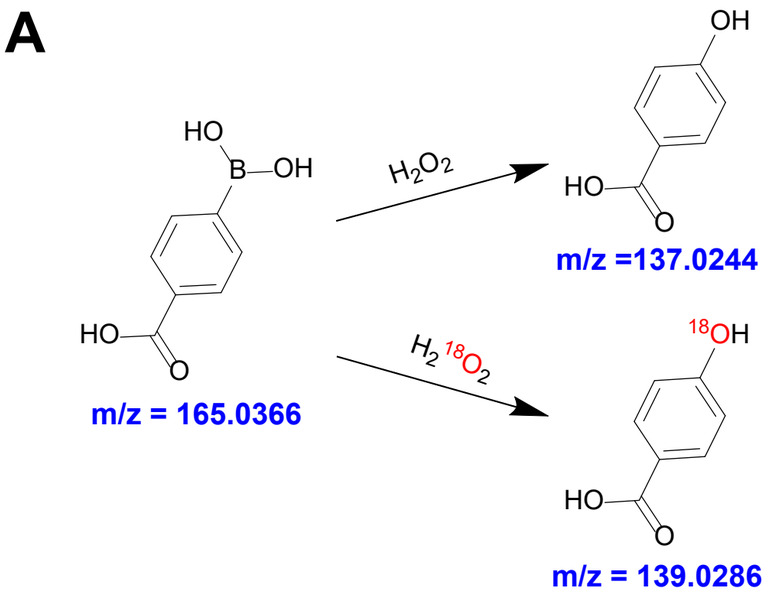
A
HO
B—OH
HO
O
m/z = 165.0366
H_2O_2
OH
HO
O
m/z =137.0244
$H_2{}^{18}O_2$
^{18}OH
HO
O
m/z = 139.0286

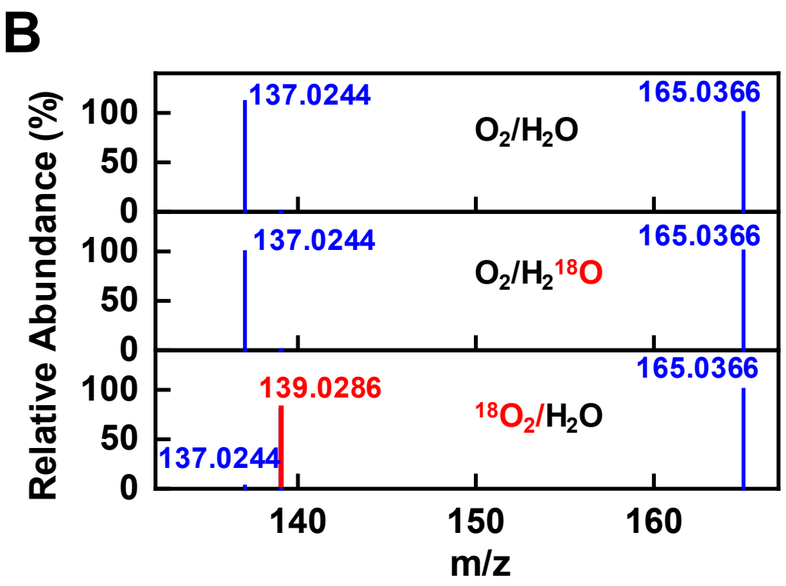
B
Relative Abundance (%)
137.0244
165.0366
O_2/H_2O
137.0244
165.0366
$O_2/H_2{}^{18}O$
139.0286
165.0366
137.0244
$^{18}O_2/H_2O$
100
50
0
140
150
160
m/z

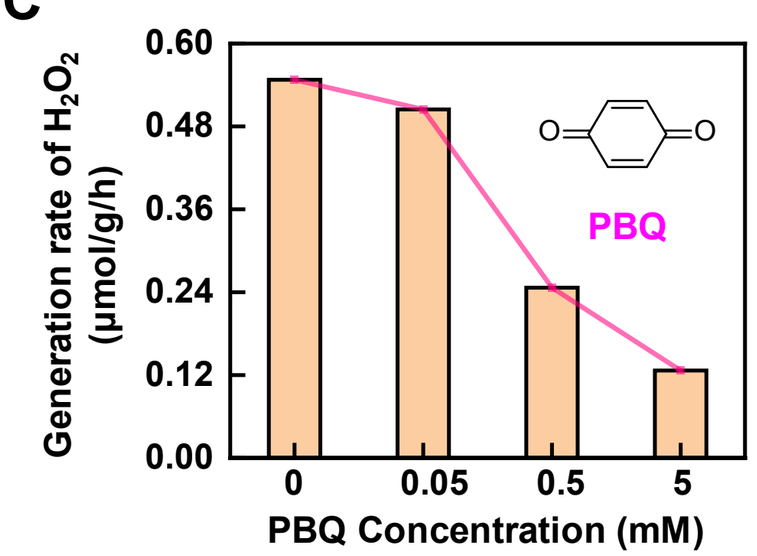
C
Generation rate of H_2O_2 (μmol/g/h)
0.60
0.48
0.36
0.24
0.12
0.00
O
O
PBQ
0
0.05
0.5
5
PBQ Concentration (mM)

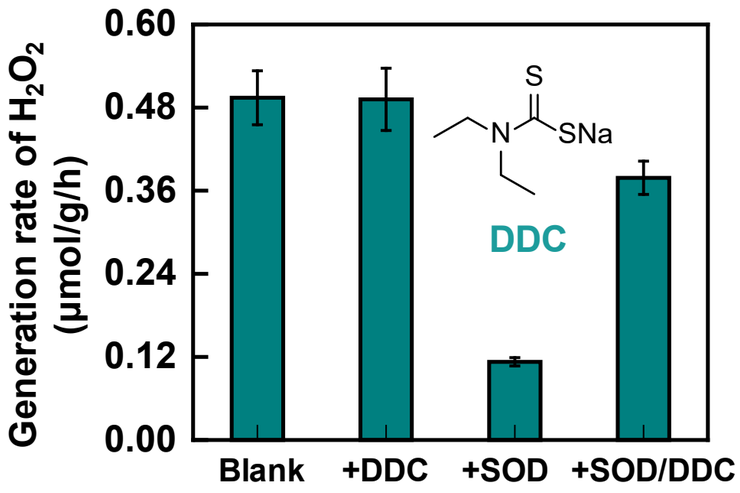
D
Generation rate of H_2O_2 (μmol/g/h)
0.60
0.48
0.36
0.24
0.12
0.00
S
N
SNa
DDC
Blank
+DDC
+SOD
+SOD/DDC

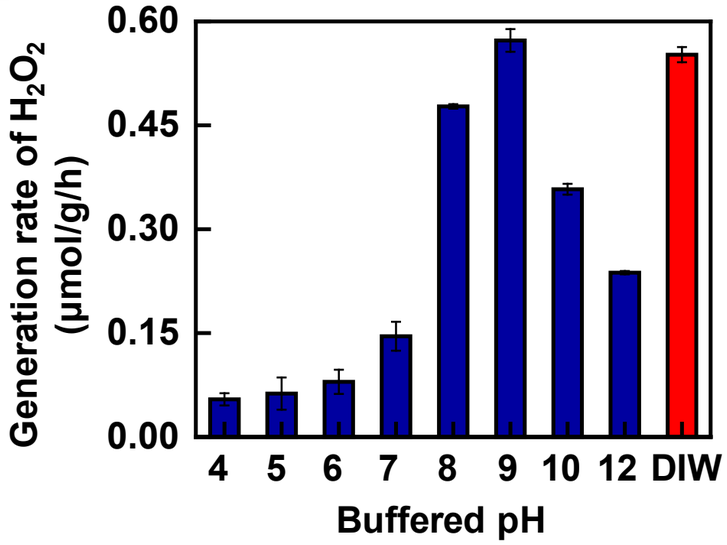
E
Generation rate of H_2O_2 (μmol/g/h)
0.60
0.45
0.30
0.15
0.00
4
5
6
7
8
9
10
12
DIW
Buffered pH

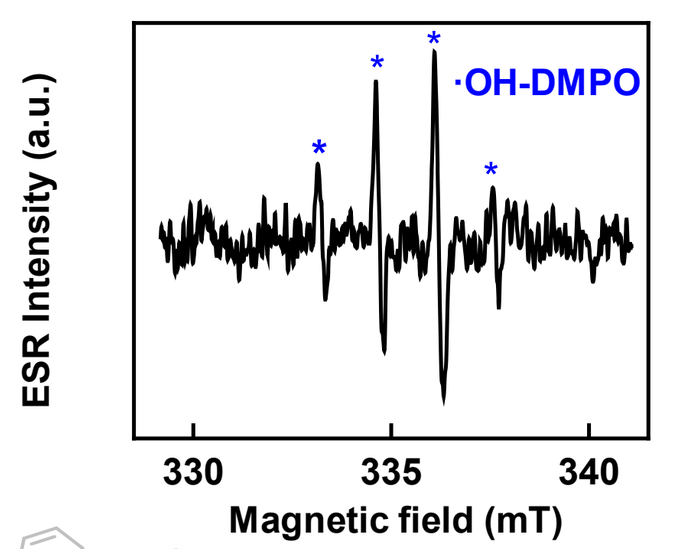
F
ESR Intensity (a.u.)
·OH-DMPO
*
330
335
340
Magnetic field (mT)

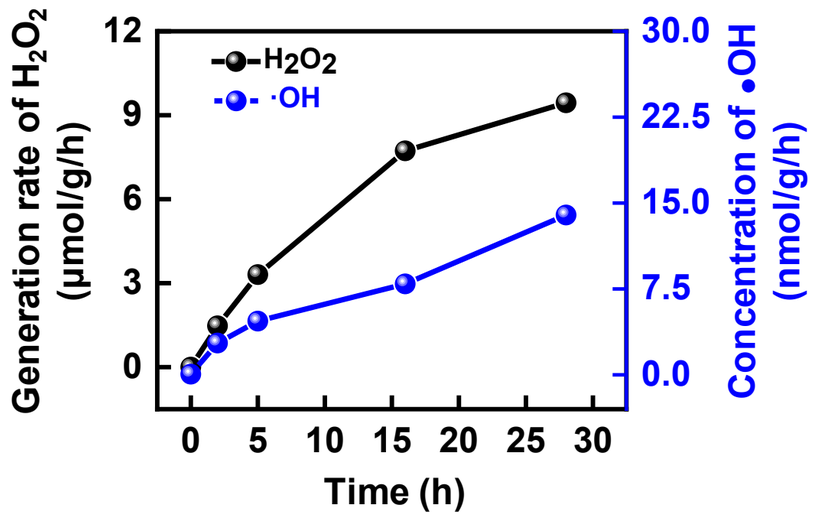
G
Generation rate of H_2O_2 (μmol/g/h)
Concentration of •OH (nmol/g/h)
H_2O_2
·OH
12
9
6
3
0
30.0
22.5
15.0
7.5
0.0
0
5
10
15
20
25
30
Time (h)

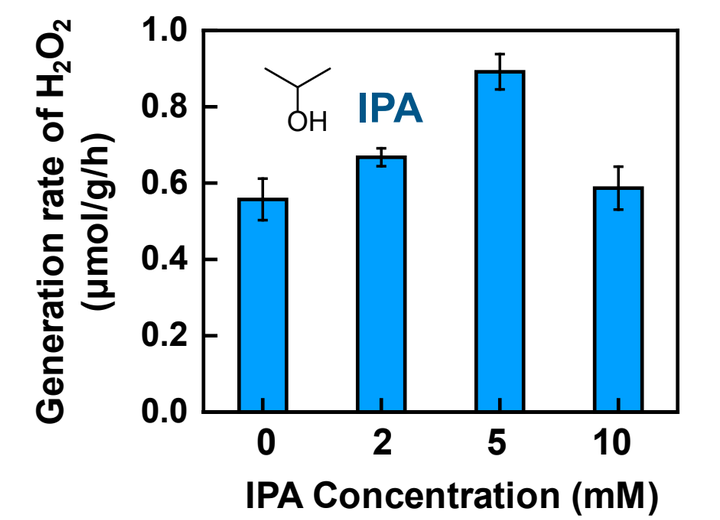
H
Generation rate of H_2O_2 (μmol/g/h)
OH
IPA
1.0
0.8
0.6
0.4
0.2
0.0
0
2
5
10
IPA Concentration (mM)

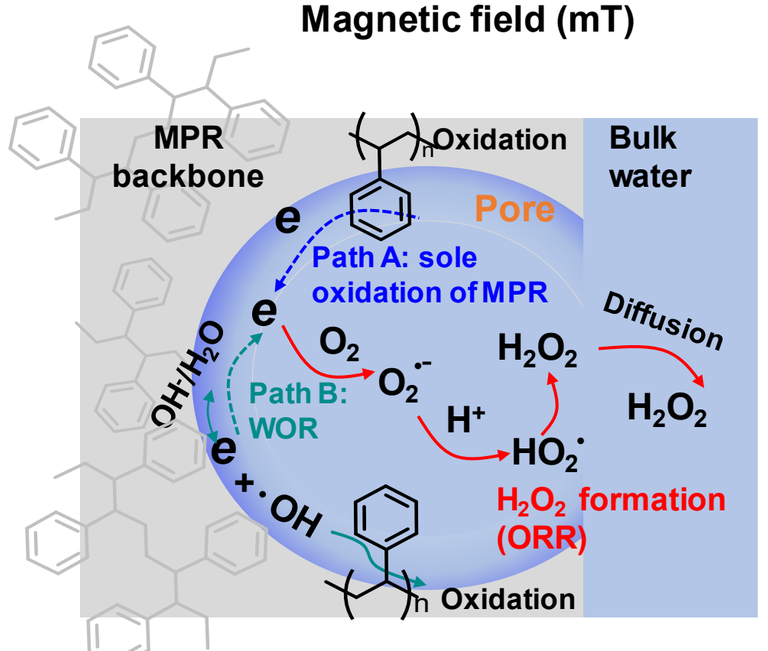
I
MPR backbone
Oxidation
Bulk water
Pore
e
Path A: sole oxidation of MPR
Diffusion
H_2O_2
O_2
$O_2^{\bullet-}$
H_2O_2
OH^-/H_2O
Path B: WOR
H^+
$HO_2^{\bullet}$
e
+·OH
H_2O_2 formation (ORR)
Oxidation

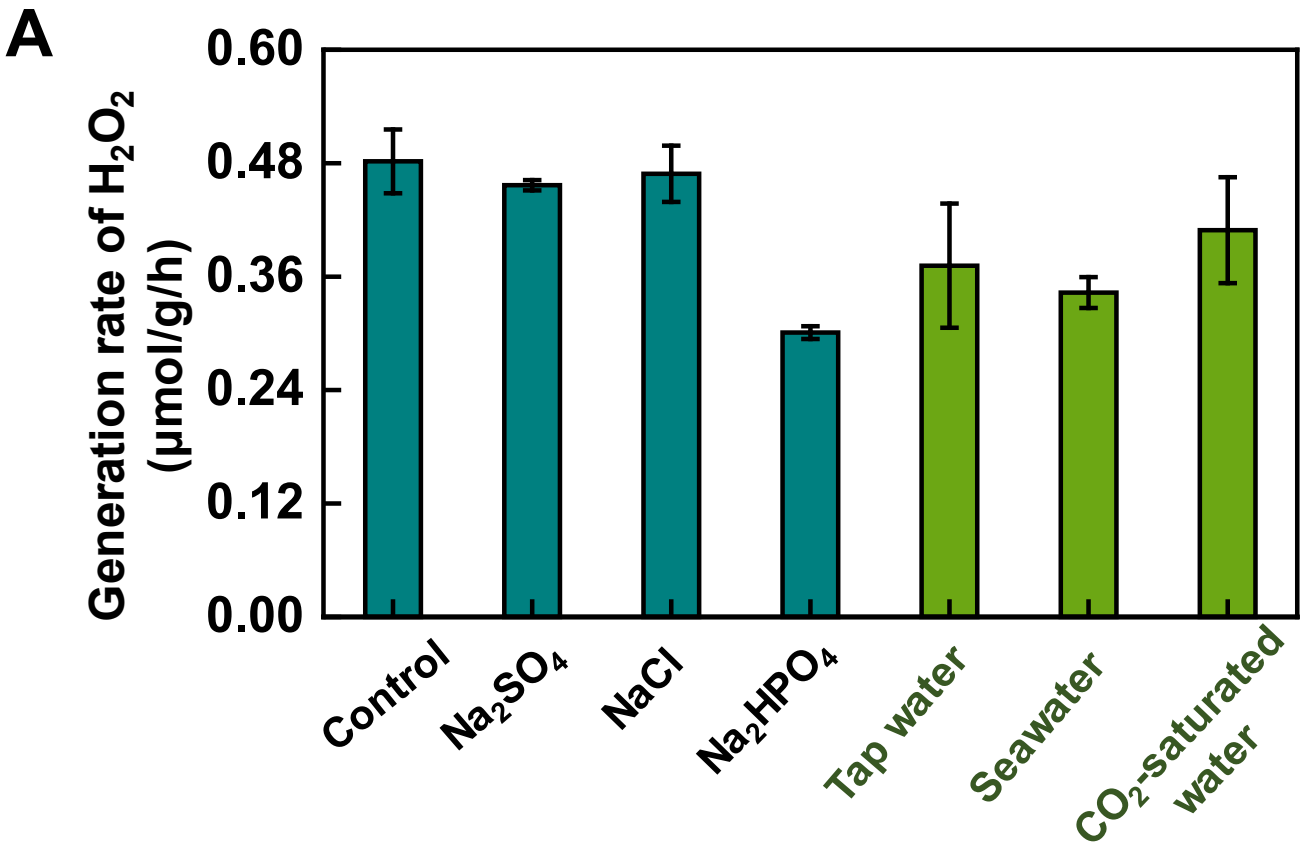
A
Generation rate of H_2O_2 (μmol/g/h)
0.60
0.48
0.36
0.24
0.12
0.00
Control
Na_2SO_4
NaCl
Na_2HPO_4
Tap water
Seawater
CO_2-saturated water

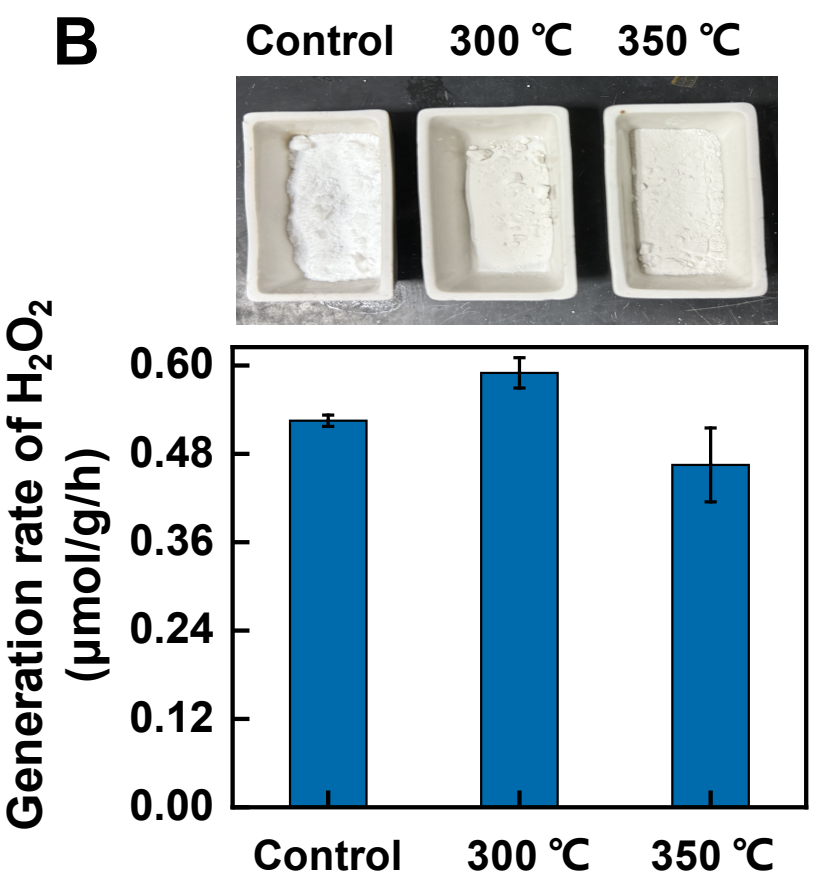
B
Control
300 ℃
350 ℃
Generation rate of H_2O_2 (μmol/g/h)
0.60
0.48
0.36
0.24
0.12
0.00
Control
300 ℃
350 ℃

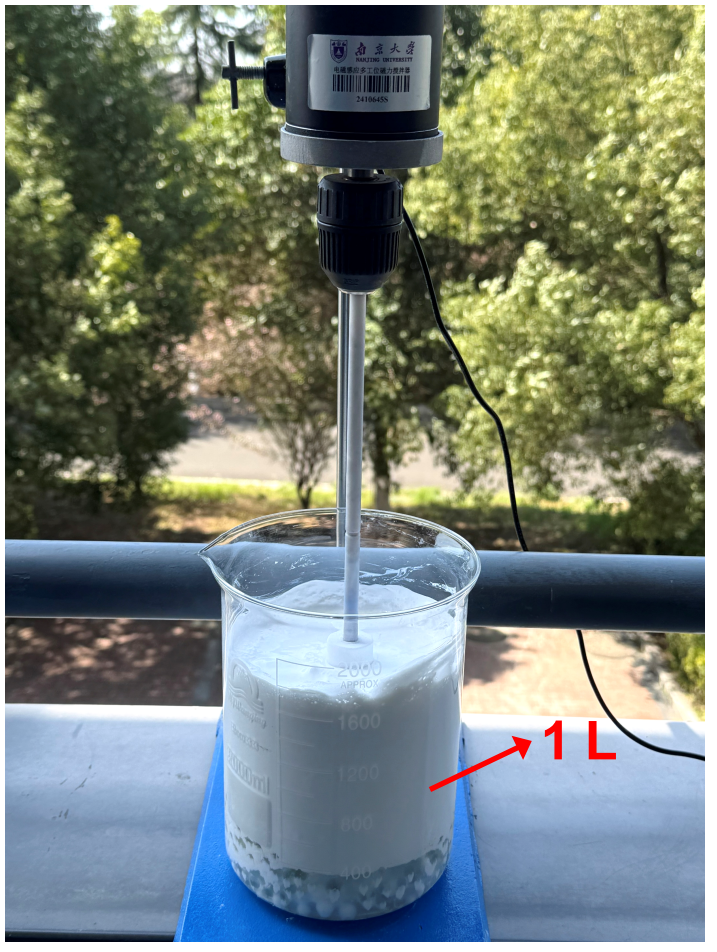
C
1 L

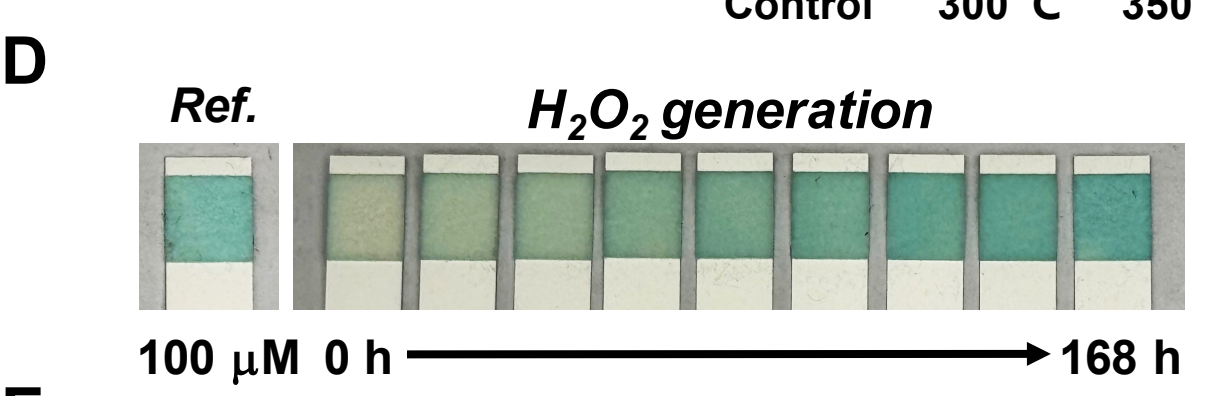
D
Ref.
H_2O_2 generation
100 μM 0 h
168 h

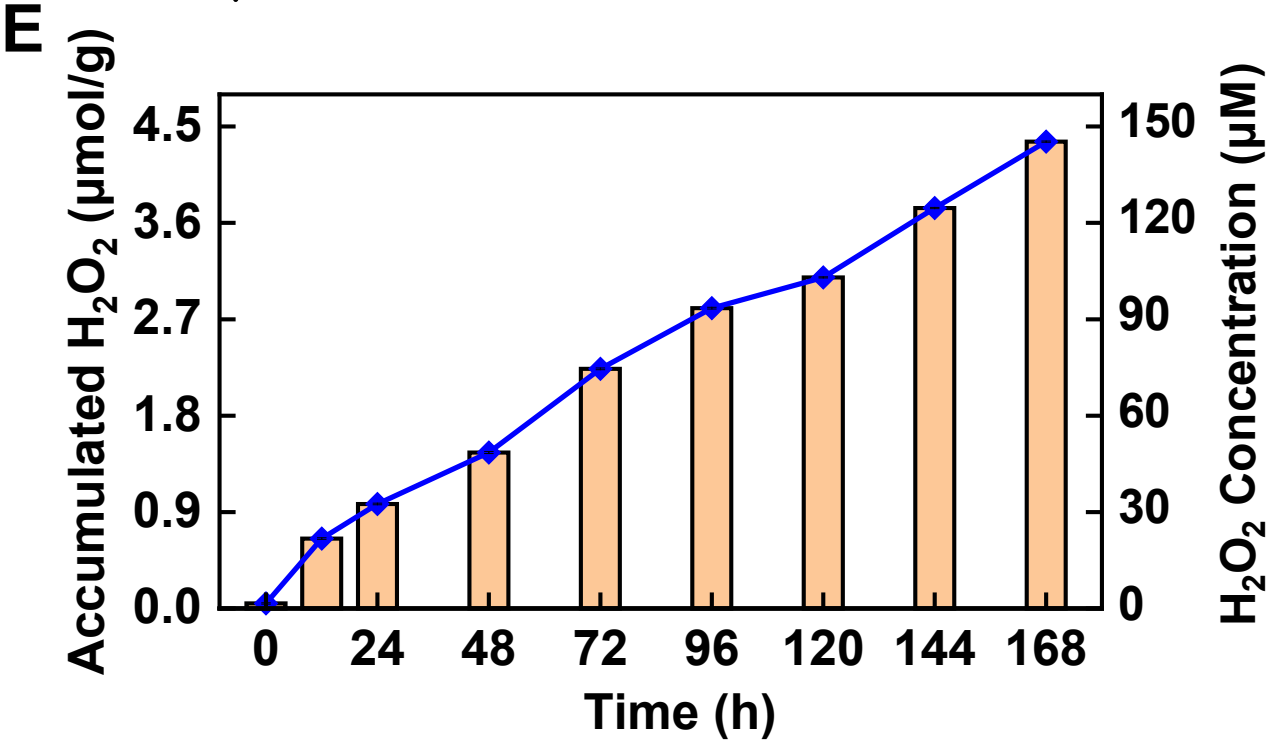
E
Accumulated H_2O_2 (μmol/g)
4.5
3.6
2.7
1.8
0.9
0.0
H_2O_2 Concentration (μM)
150
120
90
60
30
0
0
24
48
72
96
120
144
168
Time (h)